(NASA-CR-158678) STUDY OF THE EFFECTS OF IMPURITIES ON THE PROPERTIES OF SILICON MATERIALS AND PERFORMANCE OF SILICON SOLAR CELL (Sah (C. T.) Associates, Urbana, Ill.) 95 p HC A05/MF A01 CSCL 10A G3/44
N79-24447
Unclas
22150

STUDY OF THE EFFECTS OF IMPURITIES ON THE PROPERTIES OF SILICON MATERIALS AND PERFORMANCE OF SILICON SOLAR CELL

SECOND TECHNICAL REPORT

March 1979

By C. T. Sah

Contract No. 954685

The JPL Low Cost Solar Array Project is sponsered by the U. S. Dept. of Energy and forms a part of the Solar Photovoltaic Conversion Program to initiate a major effort toward the development of low-cost solar arrays. This work was performed for the Jet Propulsion Laboratory, California Institute of Technology by agreement between NASA and DOE.

DOE/JPL-954685-79/1
Dist. Category UC-63

STUDY OF THE EFFECTS OF IMPURITIES ON THE PROPERTIES OF SILICON MATERIALS AND PERFORMANCE OF SILICON SOLAR CELL

SECOND TECHNICAL REPORT

March 1979

By C. T. Sah

Contract No. 954685

The JPL Low Cost Solar Array Project is sponsered by the U. S. Dept. of Energy and forms a part of the Solar Photovoltaic Conversion Program to initiate a major effort toward the development of low-cost solar arrays. This work was performed for the Jet Propulsion Laboratory, California Institute of Technology by agreement between NASA and DOE.

TECHNICAL CONTENT STATEMENT

NEW TECHNOLOGY

No new technology is reportable for the period covered by this report.

TABLE OF CONTENT

LIST OF ILLUSTRATIONS

LIST OF TABLES

LIST OF TABLES
(continued)

ABSTRACT

This program is conducted to study the effects of impurities and defects on the performance and permanence of silicon solar cells both theoretically using computer models and experimentally.

Numerical solutions are obtained from the exact one dimensional transmission line circuit model to study the following effects on the terrestrial performance of silicon solar cells: (i) interband Auger recombination, (ii) surface recombination at the contact interfaces, (iii) enhanced metallic impurity solubility, (iv) diffusion profiles, and (v) defect-impurity recombination centers. Thermal recombination parameters of titanium impurity in silicon are estimated from recent experimental data. Based on these parameters, computer model calculations show that titanium concentration must be kept below 6×10^{12} Ti/cm^3 in order to achieve 16% AM1 efficiency in a p+/n/n+ silicon solar cell of 250 μm thick and 1.5 ohm-cm resistivity or 5×10^{15} donors/cm^2.

Computer studies of 10 ohm-cm high efficiency p+/n/n+ silicon solar cells give the following indications. (i) Interband Auger recombination is unimportant in both the diffused emitter and back surface field layers even if experimental interband Auger recombination rates used in the computer model are in error and too small by a factor of 100. (ii) Interface recombination at the front and back surfaces cannot be important unless the interface recombination velocities lie between the diffusion velocity, 10^5 cm/s, and the effective recombination velocity, 10^3 cm/s, in the diffused emitter or back surface field layer. (iii) The difference in cell performance between the Gaussian and the measured boron and phosphorus diffusion profiles is negligible. (iv) Enhanced solubility of recombination centers in the diffused emitter will decrease the short circuit current, while in the back surface field layer, it will decrease the open circuit voltage. 15% reduction can be expected if the solubility of the recombination center is 10% of the diffusion impurities in these layers. (v) A similar reduction can occur if the boron related impurity-vacancy recombination center is present in the boron diffused emitter or if the phosphorus-vacancy (E-center) recombination center is present in the phosphorus diffused back surface field layer. (vi) Analysis of the experimental data of Sandia high efficiency back surface field cells shows that either a 1% gold or 0.1% phosphorus-vacancy recombination center in the back surface field layer can account for the observed 16.8% AM1 efficiency, 620 mV open circuit voltage and 30 mA/cm^2 short circuit current. The maximum attainable AM1 efficiency of this cell design is 19.26% if both the emitter and back surface field layer recombinations are negligible and base lifetime is 700 μs.

Analyses of diffusion length, lifetime and transient capacitance data of Ti-doped silicon crystals and silicon solar cells indicate that there are three recombination levels. The two lower levels, E_V+336 and E_C-470 mV, are donor like and Ti related while the upper level, E_C-182, is a complex center containing possible oxygen, vacancy and carbon. Thermal capture and emission rates at these Ti levels are estimated from these experimental data.

1. INTRODUCTION

The objective of this program is to determine the effects of impurities and defects on the performance and permanence of silicon solar cells. It includes theoretical (computer model) and experimental studies of the effects of impurities on the properties of silicon intentionally doped with specific impurity elements, as well as the effects of these impurities on the impurity related energy levels, concentration of these energy levels and recombination-generation properties of electrons and holes at these energy levels.

This second technical report contains extension of the theoretical and computer analyses of silicon solar cell performance reported in the first technical report.[1] New factors considered are: diffusion profiles of the emitter and back surface field layers, interband Auger recombination, and band-bound thermal recombination localized at the impurity and defect-impurity centers whose solubilities are enhanced in the diffused emitter and back surface field layers. A detailed analysis of the recombination properties of the Ti impurity is also made by combining Northrop's diffusion length data, Westinghouse's concentration and OCD lifetime data and our preliminary transient capacitance data. These recombination parameters are then used to compute the theoretical solar cell performance which is then compared with the experimental AM1 performance of Ti-doped n+/p and p+/n silicon cells without anti-reflection coating reported by Westinghouse. Projection of the maximum allowable Ti concentration for a given AM1 efficiency is computed for the highest efficiency cell structure, the anti-reflection coated p+/n/n+ diode. To achieve 16% AM1 efficiency, Ti concentration must be kept below about $6\text{x}10^{12}$ Ti/cm^3.

Due to the large number of variables and parameters considered in the theoretical models and two types of recombination models used in the high efficiency cells and Ti-doped cells, the following format will be used in the presentation of the results. The format within each chapter is similar to that used in the first technical report.[1] The technical discussion are given here in two chapters, 2 and 3. Chapter 2 covers the high efficiency cell which is used to analyze the effects of diffusion profiles and Auger recombination mechanism. Chapter 3 covers the Ti-doped cells and a projection of maximum allowed Ti concentration. Section titles and starting page numbers are given below.

2. TECHNICAL DISCUSSION - HIGH EFFICIENCY CELLS

2. TECHNICAL DISCUSSION - HIGH EFFICIENCY CELLS

2.0 Objectives

The purpose of these numerical calculations is to determine the effects of emitter and back-surface-field (BSF) recombination on the efficiency (EFF), open circuit voltage (VOC), short circuit current (JSC), and fill factor (FF), as well as the position dependent internal characteristics of silicon solar cells. The internal characteristics studied include the steady-state carrier concentration, recombination rates, lifetimes, impurity charge states, electric field, electrostatic potential and diffusion, drift and recombination currents. The position variations of these internal characteristics are particularly valuable for a fundamental understanding of the effects of impurity on cell performance.[1]

The study covered in this chapter includes the effects of interband Auger recombination in the high-concentration diffused emitter and BSF layers, the enhanced solubility of recombination impurities in these layers, the presence of defect-impurity pairs or higher order complexes as electron-hole recombination sites, as well as the shape of the majority impurity (boron, phosphorus and arsenic) diffusion profile on the recombination currents.

2.1 Approach

The transmission line circuit model will be used in the numerical solution to give the cell performance characteristics. A one dimensional model is used so that the solutions are the maximum achievable since lateral losses and two and three dimensional inhomogeneities are not included. The transmission line method is particularly advantageous for device physics analysis since the physical mechanisms, such as diffusion, recombination, optical generation and boundary conditions at the contacts, are directly represented by circuit elements (resistance, capacitance, dependent and independent current sources) in the model. Thus, variations of these physical mechanisms can be readily made by modification of the circuit elements. In addition, the transmission line circuit model can be solved numerically by the well-known and highly developed and efficient matrix techniques which are available in many scientific computer languages. The details of the logical and computational sequence of solutions were described in the first technical report, (TR-1, section 2.1.3)[1] and will not be repeated here. Modifications and improvements will be described in detail here in the following subsections.

2.1.1 Recombination Models

The coupled gold donor-acceptor recombination center is used as the recombination model to study the effects of BSF, interband Auger recombination and enhanced solubility in subsections 2.2, 2.3 and 2.4. In section 2.5, a single level acceptor from the phosphorus-vacancy pair (PV) is used as the recombination model in the phosphorus diffused BSF and a single level donor complex, involving vacancies and unidentified impurities, is used as the recombination model in the boron diffused emitter. The recombination parameters of these centers are given in the tables below.

Table 2.1 Recombination Parameters at the Gold Center in Silicon at 297K.[1]

Acceptor Level			Lifetime at 10^{14} Au/cm^3
c_{n0} =	.30000E-08	cm^3/sec	τ_{n0} = 3.333 μs
e_{n1} =	.88500E+03	1 /sec	
c_{p1} =	.13743E-06	cm^3/sec	τ_{p1} = 72.76 ns
e_{p0} =	.50000E+02	1 /sec	
E_T-E_I =	.85710E-01	eV	
E_T =	E_C - 547.23	meV	
Donor Level			
c_{p0} =	.55948E-07	cm^3/sec	τ_{p0} =178.7 ns
e_{p-1} =	.17500E+08	1 /sec	
c_{n-1} =	.61200E-07	cm^3/sec	τ_{n-1} =163.4 ns
e_{n0} =	.21000E-01	1 /sec	
E_T-E_I =	-.26400E-00	eV	
E_T =	E_V + 355.66	meV	

Table 2.2 Recombination Parameters at the Donor Level in Boron Diffused Layer in Silicon at 297K.

Donor Level				Lifetime at 10^{14} Levels/cm^3		
c_{p0}	=	.18194E-07	cm^3/sec	τ_{p0}	=	549.45 ns
e_{p-1}	=	.23205E+06	1 /sec			
c_{n-1}	=	.11700E-05	cm^3/sec	τ_{n-1}	=	8.547 ns
e_{n0}	=	.98460E+01	1 /sec			
$E_T - E_I$	=	-.18211E+00	eV			
E_T	=	E_V + 354	meV			

Table 2.3 Recombination Parameters at the Phosphorus-Vacancy (PV) Acceptor Level in Phosphorus Diffused Layer in Silicon at 297K.

Acceptor Level				Lifetime at 10^{14} PV/cm^3		
c_{n0}	=	.27660E-06	cm^3/sec	τ_{n0}	=	36.153 ns
e_{n1}	=	.78330E+05	1 /sec			
c_{p1}	=	.20000E-05	cm^3/sec	τ_{p1}	=	5.000 ns
e_{p0}	=	.75320E+03	1 /sec			
$E_T - E_I$	=	.84827E-01	eV			
E_T	=	E_C - 471.6	meV			

The data given in the above two tables are obtained from voltage stimulated transient capacitance measurements (VSCAP) on one-MeV electron irradiated Si diodes. Detailed descriptions on how these parameters were obtained are given in section 2.5 (page 46) where they are used in the computer calculations.

The coupled gold donor-acceptor recombination center was also used in TR-1. For high efficiency silicon solar cells and silicon devices with long recombination lifetimes, the residue recombination center is likely to be gold due to gold contamination during the device processing steps. The two-level gold recombination center is also a good model for other possible residue metallic impurities in terrestrial silicon solar cells made from low-cost silicon.

Experimental evidence from phosphorus diffusion profile studies has indicated that the phosphorus-vacancy center is necessary to explain the non-complementary error function or non-Gaussian phosphorus diffusion profiles.[2] A similar defect or defect-impurity cluster with a donor charge state may be present in the study of the boron diffusion profile in silicon.[3] Although these diffusion profile studies and models by no means indicate the presence of these two centers, they will be employed to determine if recombination at these centers will limit the ultimate efficiency of silicon solar cells when all other impurity recombination centers are eliminated.

In order to simulate the experimental high efficiency silicon solar cells produced by Sandia Corporation,[4] the concentration of the recombination centers in the quasi-neutral base region is selected so that the open circuit midbase lifetime is equal to the reported value, 700 μs, in the high-efficiency Sandia P+/N/N+ cells. For the gold model, this lifetime corresponds to a gold concentration of $4.465\text{x}10^{10}$ Au/cm^3, an extremely low value.

The interband Auger recombination mechanism is also included in the computer calculations since it was thought that Auger recombination may be important. The interband Auger recombination rates are from experimental data.[5] The impact ionization rates are computed from mass action law $e^n=c^n n_i^2$ and $e^p=c^p n_i^2$ where $n_i(297)=1.036\text{x}10^{10}$. The interband Auger capture rates and their inverse or impact generation rates are given in the following table.

Table 2.4 Interband Auger Recombination and Impact Generation Rate of Electron-Hole Pairs by Electrons and Holes in Silicon at 297K.

$c^n = 2.8 \times 10^{-31}$ cm^6/sec

$e^n = 3.0 \times 10^{-11}$ 1 /sec

$c^p = 9.9 \times 10^{-32}$ cm^6/sec

$e^p = 1.06 \times 10^{-11}$ 1 /sec

$n_i = 1.036 \times 10^{10}$ 1 /cm^3

Lifetime at 10^{18} carrier/cm^3

$\tau_p = 2.6$ μs

$\tau_n = 10.1$ μs

Other complicating factors are not included in the computer model, following the reasons given in TR-1.[1] There are two considerations, one concerns the fundamental material physics and the other the availability of reliable data.

Energy gap narrowing and Fermi-Dirac statistics are both excluded in the model for a number of fundamental reasons given below. (i) Energy gap narrowing has been attributed to high impurity density which gives rise to random impurity potentials. These random potentials perturb the band states into the band gap to form the so-called band tail and gap states. However, these band tail and gap states are highly localized at the impurity sites. They are recombination or trapping states with nearly zero or very low mobilities and hence cannot be treated in the same way as the high mobility band states. Thus, they do not contribute to energy gap narrowing in the way that is taken into account in the literature where an effective intrinsic carrier density, n_i, is used which depends on an effective energy gap that includes narrowing. Such a treatment tacitly assumes that band tail states are high mobility states but they are not. (ii) Localized statistics for bound state energy levels,[7] instead of Fermi-Dirac statistics for band states, must be used to determine the electron or hole occupation at these localized band tail states. (iii) Deionization of the shallow energy level impurities (phosphorus, arsenic and boron) must be taken into account at high carrier concentrations. (iv) Impurity banding must also be taken into account at high impurity concentrations when inter-impurity distance becomes comparable to the bound state orbital diameter.

Although energy gap narrowing, Fermi-Dirac statistics, impurity deionization and impurity band formation are excluded in the computer model, their effects on solar cell performance tend to compensate each other, resulting in a much smaller net contribution. This compensation effect also makes the experimental separation of their influences very difficult.

To illustrate the compensation effect, we note that energy gap narrowing will increase the minority carrier density and hence increase the recombination current. However, Fermi-Dirac statistics will decrease the minority carrier density and hence decrease the minority carrier recombination current.

As another illustration, impurity deionization and banding will decrease the majority carrier concentration and hence increase the minority carrier concentration, recombination rate and current. However, reduction of the majority carrier concentration will reduce the Debye screening of the electron-hole Coulombic interaction. Debye screening of the electron-hole attraction is the cause of real energy gap narrowing since it involves no bound states and only band electrons and holes. Thus, smaller Debye screening due to lower majority carrier density from impurity deionization would lessen energy gap narrowing and hence decrease the recombination rate and current.

Aside from the fundamental considerations given above which indicate that the net effect of the four factors we neglected (energy gap narrowing, Fermi-Dirac statistics, impurity deionization and impurity banding) is small, there are also several experimental indications which are not inconsistent with the contention that their net effect is small. First, there is no reliable and consensus experimental data on energy gap narrowing. Some recently reported data were subsequently proved to be inaccurate. Second, silicon solar cell performance data (efficiency, VOC, JSC) of the best high-efficiency cells are already nearly equal to the theoretically computed maximum values without the inclusion of energy gap narrowing, Fermi-Dirac statistics, impurity deionization and impurity banding. The lack of reliable experimental data suggests that the factors are compensating so that it is difficult to isolate them out individually from experimental data. The good agreement between theory and experiments on the best high efficiency silicon solar cells again suggests that these factors are compensating or individually unimportant.

2.1.2 Computer Model

Numerical computations are made using the transmission line equivalent circuit model method described in section 2.1 of Technical Report No. 1. The circuit model was synthesized from the exact Shockley Equations. Hence, the results are exact with only numerical inaccuracy which is much less than 1%. The only changes made are in the computer model and the numerical integration scheme for the photocurrent generators.

The computer model and the numerical integration scheme for the photocurrent employed in this chapter give slightly better accuracy than those employed in T.R. No. 1. The computer model is again a four region model consisting of the emitter region, the junction space charge region, the quasi-neutral base and the back surface field region. A two hundred (198) section model is used in which the section numbers of the four regions are 25, 50, 73 and 25 in contrast to 20/60/91/25 used in TR-1. The emitter region thickness is taken to equal the emitter junction depth, $0.25\text{x}10^{-4}$ cm. The emitter space charge region is chosen to be $0.75\text{x}10^{-4}$ cm which insures that it will cover the entire transition region of rapidly changing electrostatic potential at equilibrium (zero applied voltage in the dark). The 'true' space charge region will always be thinner than this second region of the 4-region model. The fourth region is made large enough to cover the entire back surface field layer. The thickness of the fourth region is set to eight times the emitter junction depth, $2.0\text{x}10^{-4}$ cm. The physical BSF layer has a thickness of $1.0\text{x}10^{-4}$ cm. The quasi-neutral base or the third region has a thickness of $300-0.25-0.75-2.0=297\text{x}10^{-4}$ cm. The cell thickness is chosen to be $300\text{x}10^{-4}$ cm to make it equal to that of the experimental high efficiency cell. The section sizes are constant except in the third or quasi-neutral base region where the size increases linearly to a peak and then decreases linearly so that the sizes of the boundary sections are identical to those of the adjacent regions, the space charge region and the back surface field region. Such a section size variation without discontinuities across the region boundaries is crucial to obtain accurate numerical solutions.

The numerical integration method for the photocurrent generators in each section has been improved over that used in TR-1. In TR-1, the Trapezoid rule was used for the double integral of integration over the position in the cell and over the wave length of the solar spectra. For the 200 μm thick cell, this gave 34.405 mA/cm^2 maximum photocurrent for the 22/60/91/25 computer model in TR-1. The exact integration over position (equivalent to ∞/∞/∞/∞ computer model) and Simpson rule integration over solar spectrum used in this report gave 33.880 mA/cm^2. Thus, the TR-1 computer model corresponded to a slightly higher solar intensity than that used in the input spectra due to the numerical error in the Trapezoid integration rule used in TR-1. We shall call 33.880 mA/cm^2 the exact value (i.e., ∞/∞/∞/∞ model) with the understanding that it is obtained by a Simpson Rule integration over wavelength which makes it still approximate but is dictated by the discrete solar spectral irradiance data.

In the new scheme, the distributed photocurrent generator in each section is evaluated by the Simpson rule over the wavelength integration and exactly over the position integration. The photocurrent generator located at position x_1 is then given by

$$qg_0(x_1)[x_2-x_1] = q\int_{\lambda_0}^{\lambda_\infty} G_1(0,\lambda)[e^{-\lambda x_1} - e^{-\lambda x_2}]d\lambda \qquad (2.1)$$

The sum of the distributed photocurrent generators over all 198 sections is equal to the exact value of 33.880 mA/cm^2 indicated above. This removes an absolute numerical error associated with the use of the Trapezoid rule for the dx integration used in TR-1.

The test of the two methods of integration on solar cell parameters is illustrated in Table 2.5. The cell is a silicon P+/N/N+ BSF cell with Auger recombination and spatially constant gold recombination density of $4.465\text{x}10^{10}$ Au/cm^3 to give an open circuit midbase steady-state lifetime of $\tau_{OC}(x=150\mu m)=700\mu s$. Measured phosphorus and boron impurity profiles were also used (see next subsection 2.1.3) which give

$$\begin{aligned} N_{AA}(Z) - N_{DD}(Z) = {} & 1.25\text{x}10^{20}[1 - (Z/L_1)^{2/3}]U(L_1-Z) \\ & - 5.0\text{x}10^{14} \\ & - 2.5\text{x}10^{20}\exp[-(L-Z)^6/L_2^6] \quad \text{Atoms/cm}^3 \end{aligned} \qquad (2.2)$$

Here, U(X) is the unit step function:

$U(L_1-Z)=1$ for $Z<L_1$ and $U(L_1-Z)=0$ for $Z>L_1$. L_1 is evaluated to give a emitter junction depth of 0.25μm. L_2 is evaluated to give a BSF layer junction of 1.0 μm from the back surface.

Table 2.5 Effect of Photogenerator on Silicon P+/N/N+ Cell Performance at one AM1 Sun

Computer Run No.	JPHOTO mA/cm^2	EFF %	VOC mV	JSC mA/cm^2	FF	Integration Method dλ	Integratio Method dx
RUN571	35.030	19.527	669.40	33.877	0.76566	Trapezoid	Trapezoid
RUN575	34.448	19.197	668.68	33.345	0.76557	Simpson	Exact

It is evident that the errors are insignificant compared with achievable experimental accuracy. However, when comparing various fundamental mechanisms using the computer results, the more accurate model given by RUN575 using the Simpson integration rule for dλ and exact integration rule for dx is preferred. CPU time was increased by much less than 1%.

2.1.3 Device and Material Parameters

The following parameters are used so that the results of this study on the various recombination effects can also be compared with published experimental data. The experimental parameters of the Sandia P+/N/N+ cells are used here. They are listed below.

Table 2.6

Item			Reference
1	$T = 297$	K	
2	$n_i = 0.10360$ E+11	$1/\text{cm}^3$	
3	$L = 300.00$	μm	4
4	$X_J = 0.25$	μm	4
5	$X_{BSF} = 1.0$	μm	4
6	$\rho_B = 10$ (n-type FZ)	Ω-cm	4
7	$C_0 = 0.125$ E+21	B/cm^3	3,4
8	$C_B = 0.500$ E+15	P/cm^3	4
9	$C_L = 0.250$ E+21	P/cm^3 or	2,4
	0.700 E+21	P/cm^3	
10	$N_B(x) = C_0[1-(x/L_1)^{2/3}]U(L_1-x_1)$	B/cm^3	3,9
11	$N_P(x) = C_L \exp[-(L-x)^6/L_2^6]$	P/cm^3	2,8

The concentration profiles of boron diffused emitter and the phosphorus diffused BSF given in items 10 and 11 of this table come from sheet resistivity measurements with anodic etching of thin layers.[2,3,8,9] The formulae given in items 10 and 11 are simple empirical fits to the experimental data given by the BTL (Bell Telephone Lab) work.[2,3] The Westinghouse boron profile[9] also fits $(1-Y^{2/3})$ reasonably well. However, the two step phosphorus profile reported by Westinghouse (and IBM)[8] and attributed to $P_xO_yN_y$ nitride layer formation is not used in this chapter but is used in chapter 3 where studies of Ti-doped Westinghouse cells are made. Both the $(1-Y^{2/3})$ boron profile and the $\exp(-Y^6)$ phosphorus profile are considerably flatter than the ideal diffusion profiles, $\exp(-Y^2)$ and erfc(Y).

Two values[2] for the phosphorus surface concentration, C_L, are used as listed in item 9. The lower value ($2.5\text{x}10^{20}$) corresponds to the electrically active phosphorus or electron concentration while the higher value ($7.0\text{x}10^{20}$) corresponds to the electrically active phosphorus donors, but ($4.5\text{x}10^{20}$) of these may be neutralized by the PV acceptors to give a net of ($2.5\text{x}10^{20}$) electrons/cm^3 if the PV pairs are electrically active.

The phosphorus surface concentrations given in item 9 and the boron surface concentration given in item 7, both from BTL work,[2,3] can also be computed from the sheet resistance measurements of Sandia[4] and Westinghouse[8,9] using a resistivity versus concentration curve[10] similar but not identical to that of Irwing's.[11] Differences occur for concentrations greater than 10^{19} cm^{-3} where our mobilities drop to constant values of $\mu_n=90$ and $\mu_p=45$ as given by Equations (2.60) and (2.61) of TR-1.

The empirical fits to the experimental diffusion profiles of phosphorus, $\exp(-Y^6)$, and boron, $(1-Y^{2/3})$, will be known as the *measured* profiles in this report.

2.1.4 Solar and Optical Parameters

The AM1 solar radiation spectrum used in this report is identical to that given on p.38 and 39 of TR-1 which come from a Table given by Thekaekara.[12] As in TR-1, the data for a particular ambient condition is used since a detailed tabulation of the AM1 solar spectrum is given. The ambient corresponds to 20mm H_2O and 3.4mm O_3 and the total incident power is 88.92 mW/cm^2. This is somewhat smaller than those used by other workers in AM1 efficiency calculations which ranged upwards to 92.46 mW/cm^2 such as the work by Fossum[13] and the Westinghouse experimental quartz iodine simulator[14] calibration by a NASA Lewis standard.

Accurate absorption curves in silicon were obtained from original publications at 291K.[1] These are fitted and interpolated at closely spaced wavelengths. The silicon surface reflection coefficient, $R(\lambda)$, is calculated from

$$R(\lambda) = \frac{4n}{(1+n)^2 + k^2} \tag{2.3}$$

Here, the wave length dependence of the index of refraction, $n(\lambda)$, and extinction coefficient, $k(\lambda)$, are read off the graphs on page B-2 and B-3 of the JPL Solar Cell Radiation Handbook of Tada and Carter.[15] Reflection is neglected in the study of high efficiency cells which have antireflection coating but included in Westinghouse bare surface cells.

These are tabulated in Table 2.7. The four significant figures listed do not imply absolute accuracy but serve as a reference in the computer model so that the numerical results will retain their relative accuracy.

Table 2.7 AM1 solar spectral irradiance, silicon absorption coefficient and silicon surface reflection coefficient as a function of photon wave length. 88.92 mW/cm^2 (Part 1, 2900-6000A)

$\lambda(\mu)$	E(eV)	$\alpha(cm^{-1})$	$P(W/m^2\mu)$	$1-R(\lambda)$
.2900D+00	.4275D+01	.2119D+07	.0000D+00	3329D-00
.2950D+00	.4203D+01	.1868D+07	.0000D+00	.3881D-00
.3000D+00	.4133D+01	.1682D+07	.4100D+01	.3881D-00
.3050D+00	.4065D+01	.1547D+07	.1140D+02	.4065D-00
.3100D+00	.4000D+01	.1424D+07	.3050D+02	.4198D-00
.3150D+00	.3936D+01	.1344D+07	.7940D+02	.4285D-00
.3200D+00	.3875D+01	.1270D+07	.2026D+03	.4366D-00
.3250D+00	.3815D+01	.1204D+07	.2695D+03	.4430D-00
.3300D+00	.3757D+01	.1151D+07	.3316D+03	.4465D-00
.3350D+00	.3701D+01	.1121D+07	.3834D+03	.4470D-00
.3400D+00	.3647D+01	.1103D+07	.4313D+03	.4465D-00
.3450D+00	.3594D+01	.1089D+07	.4492D+03	.4412D-00
.3500D+00	.3543D+01	.1066D+07	.4805D+03	.4330D-00
.3550D+00	.3493D+01	.1050D+07	.4980D+03	.4250D-00
.3600D+00	.3444D+01	.1003D+07	.5137D+03	.4180D-00
.3650D+00	.3397D+01	.8838D+06	.5613D+03	.4136D-00
.3700D+00	.3351D+01	.6194D+06	.6035D+03	.4137D-00
.3750D+00	3307D+01	.4419D+06	.6094D+03	.4220D-00
.3800D+00	.3263D+01	.2979D+06	.6080D+03	.4389D-00
.3850D+00	.3221D+01	.2044D+06	.6098D+03	.4575D-00
.3900D+00	.3179D+01	.1532D+06	.6239D+03	.4742D-00
.3950D+00	.3139D+01	.1242D+06	.6912D+03	.4900D-00
.4000D+00	.3100D+01	.9596D+05	.8499D+03	.5040D-00
.4050D+00	.3062D+01	.7453D+05	.9928D+03	.5150D-00
.4100D+00	.3024D+01	.6389D+05	.1074D+04	.5256D-00
.4150D+00	.2988D+01	.5903D+05	.1105D+04	.5355D-00
.4200D+00	.2952D+01	.5619D+05	.1104D+04	.5459D-00
.4250D+00	.2918D+01	.5341D+05	.1087D+04	.5540D-00
.4300D+00	.2884D+01	.4840D+05	.1068D+04	.5614D-00
.4350D+00	.2851D+01	.4111D+05	.1100D+04	.5685D-00
.4400D+00	.2818D+01	.3399D+05	.1216D+04	.5750D-00
.4450D+00	.2786D+01	.2901D+05	.1310D+04	.5806D-00
.4500D+00	.2755D+01	.2675D+05	.1388D+04	.5859D-00
.4550D+00	.2725D+01	.2454D+05	.1435D+04	.5912D-00
.4600D+00	.2696D+01	.2238D+05	.1452D+04	.5958D-00
.4650D+00	2667D+01	.2026D+05	.1451D+04	.5997D-00
.4700D+00	.2638D+01	1819D+05	.1451D+04	.6035D-00
.4750D+00	.2610D+01	.1616D+05	.1470D+04	.6066D-00
.4800D+00	.2583D+01	.1493D+05	.1503D+04	.6097D-00
.4850D+00	.2557D+01	.1419D+05	.1443D+04	.6125D-00
.4900D+00	.2531D+01	.1342D+05	.1435D+04	.6152D-00
.4950D+00	.2505D+01	.1265D+05	.1454D+04	.6176D-00
.5000D+00	.2480D+01	.1202D+05	.1451D+04	.6200D-00
.5050D+00	.2455D+01	.1143D+05	.1440D+04	.6220D-00
.5100D+00	.2431D+01	.1081D+05	.1417D+04	.6240D-00
.5150D+00	.2408D+01	.1020D+05	.1385D+04	.6262D-00
.5200D+00	.2385D+01	.9691D+04	.1390D+04	.6281D-00
.5250D+00	.2362D+01	.9237D+04	.1410D+04	.6300D-00
.5300D+00	.2340D+01	.8833D+04	.1407D+04	.6321D-00
.5350D+00	.2318D+01	.8483D+04	.1394D+04	.6338D-00
.5400D+00	.2296D+01	.8125D+04	.1372D+04	.6352D-00
.5450D+00	.2275D+01	.7704D+04	.1354D+04	.6372D-00
.5500D+00	.2254D+01	.7290D+04	.1337D+04	.6388D-00
.5550D+00	.2234D+01	.7010D+04	.1336D+04	.6400D-00
.5600D+00	.2214D+01	.6771D+04	.1319D+04	.6411D-00
.5650D+00	.2195D+01	.6525D+04	.1330D+04	.6426D-00
.5700D+00	.2175D+01	.6255D+04	.1338D+04	.6437D-00
.5750D+00	.2156D+01	.5991D+04	.1347D+04	.6448D-00
.5800D+00	.2138D+01	.5779D+04	.1347D+04	.6458D-00
.5850D+00	.2120D+01	.5596D+04	.1347D+04	.6469D-00
.5900D+00	.2102D+01	.5416D+04	.1341D+04	.6477D-00
.5950D+00	.2084D+01	.5208D+04	.1329D+04	.6486D-00
.6000D+00	.2067D+01	.4999D+04	.1320D+04	.6497D-00

Table 2.7. AM1 solar spectral irradiance, silicon absorption coefficient and silicon surface reflection coefficient as a function of photon wave length. 88.92 mW/cm^2 (Part 2, 6000-12640A)

$\lambda(\mu)$	E(eV)	$\alpha(\mathrm{cm}^{-1})$	$P(W/m^2\mu)$	$1-R(\lambda)$
.6000D+00	.2067D+01	.4999D+04	.1320D+04	.6497D-00
.6050D+00	.2050D+01	.4795D+04	.1311D+04	.6503D-00
.6100D+00	.2033D+01	.4627D+04	.1308D+04	.6512D-00
.6200D+00	.2000D+01	.4300D+04	.1294D+04	.6529D-00
.6300D+00	.1968D+01	3982D+04	.1281D+04	.6543D-00
.6400D+00	.1937D+01	.3675D+04	.1272D+04	.6559D-00
.6500D+00	.1908D+01	.3377D+04	.1257D+04	.6571D-00
.6600D+00	.1879D+01	.3130D+04	.1244D+04	.6587D-00
.6700D+00	.1851D+01	.2906D+04	.1227D+04	.6600D-00
.6800D+00	.1823D+01	.2714D+04	.1210D+04	.6607D-00
.6900D+00	.1797D+01	.2529D+04	.1196D+04	.6620D-00
.6980D+00	.1776D+01	.2385D+04	.1010D+04	.6632D-00
.7000D+00	.1771D+01	.2350D+04	.1175D+04	.6638D-00
.7100D+00	.1746D+01	.2179D+04	.1157D+04	.6648D-00
.7200D+00	.1722D+01	.2033D+04	.1135D+04	.6660D-00
.7280D+00	.1703D+01	.1920D+04	.1003D+04	.6670D-00
.7300D+00	.1699D+01	.1892D+04	.1118D+04	.6672D-00
.7400D+00	.1676D+01	.1754D+04	.1095D+04	.6679D-00
.7500D+00	.1653D+01	.1620D+04	.1077D+04	.6690D-00
.7620D+00	.1627D+01	.1464D+04	.7940D+03	.6701D-00
.7700D+00	.1610D+01	.1362D+04	.1039D+04	.6705D-00
.7800D+00	.1590D+01	.1259D+04	.1019D+04	.6710D-00
.7900D+00	.1570D+01	.1178D+04	.1000D+04	.6726D-00
.8000D+00	.1550D+01	.1100D+04	.9812D+03	.6735D-00
.8060D+00	.1538D+01	.1044D+04	.8744D+03	.6738D-00
.8250D+00	.1503D+01	.8744D+03	.9316D+03	.6746D-00
.8300D+00	.1494D+01	.8358D+03	.9218D+03	.6750D-00
.8350D+00	.1485D+01	.8000D+03	.9124D+03	.6752D-00
.8460D+00	.1466D+01	.7228D+03	.4762D+03	.6758D-00
.8600D+00	.1442D+01	.6306D+03	.5064D+03	.6766D-00
.8700D+00	.1425D+01	.5709D+03	.4538D+03	.6771D-00
.8750D+00	.1417D+01	.5416D+03	.4492D+03	.6774D-00
.8870D+00	1398D+01	.4738D+03	.4486D+03	.6780D-00
.9000D+00	.1378D+01	.4132D+03	.4489D+03	.6784D-00
.9070D+00	.1367D+01	3813D+03	.4552D+03	6788D-00
.9150D+00	.1355D+01	.3455D+03	.4615D+03	.6791D-00
.9250D+00	.1341D+01	.3053D+03	.2790D+03	.6795D-00
.9300D+00	.1333D+01	.2866D+03	.2218D+03	.6797D-00
.9400D+00	.1319D+01	.2497D+03	.3134D+03	.6800D-00
.9500D+00	.1305D+01	.2136D+03	.2965D+03	.6805D-00
.9550D+00	.1298D+01	.1968D+03	.3211D+03	.6807D-00
.9650D+00	.1285D+01	.1699D+03	.3444D+03	.6810D-00
.9750D+00	.1272D+01	.1435D+03	.5769D+03	.6813D-00
.9850D+00	.1259D+01	.1177D+03	.5446D+03	.6813D-00
.1018D+01	.1218D+01	.5200D+02	.6175D+03	.6827D-00
.1082D+01	.1146D+01	.6568D+01	.5129D+03	.6842D-00
.1094D+01	.1133D+01	.4750D+01	.4641D+03	.6845D-00
.1098D+01	.1129D+01	.4210D+01	.5037D+03	.6847D-00
.1101D+01	.1126D+01	.3850D+01	.5048D+03	6848D-00
.1128D+01	.1099D+01	.1600D+01	.1351D+03	.6850D-00
.1131D+01	.1096D+01	.1460D+01	.1522D+03	.6852D-00
.1137D+01	.1090D+01	.1150D+01	.1431D+03	.6853D-00
.1144D+01	.1084D+01	.8800D+00	.1912D+03	.6854D-00
.1147D+01	.1081D+01	.7600D+00	.1745D+03	.6855D-00
.1178D+01	.1053D+01	.6200D-01	.3993D+03	.6860D-00
.1189D+01	.1043D+01	.2500D-01	.4022D+03	.6861D-00
.1193D+01	.1039D+01	.1900D-01	.4240D+03	.6862D-00
.1222D+01	.1015D+01	.4000D-02	.3918D+03	.6866D-00
.1236D+01	.1003D+01	.2000D-02	.3908D+03	.6869D-00
.1264D+01	.9810D+01	.0000D-00	.3292D+03	6873D-00

The dependence of the maximum photocurrent or areal photon density absorbed per second on the sample thickness is a very useful parameter in measuring the performance of an experimental solar cell and in projecting probable further improvement of a particular technology. For these reasons, the results of the Simpson rule integration of $d\lambda$ and exact integration of dx is given in the following table for silicon at one AM1 sun. Reflection at the silicon surface is neglected.

Table 2.8 Maximum Photocurrent as a Function of Silicon Solar Cell Thickness

L (μm)	JPHOTO (mA/cm^2)
0.1	3.1318
0.2	4.7755
0.5	8.1773
1.0	11.812
2.0	16.219
5.0	22.296
10.0	26.208
20.0	29.088
50.0	31.491
100.0	32.772
150.0	33.438
200.0	33.880
300.0	34.453
400.0	34.826
500.0	35.101
1000.0	35.943
2000.0	36.839
5000	37.702
10000	37.971
∞	40.853

The difference of 0.005 mA/cm^2 between the L=300μm result (34.453 mA/cm^2) and that given in Table 2.5 of RUN575 (34.448 mA/cm^2) comes from neglecting the photon flux in the last $d\lambda$ at the absorption threshold. It should be mentioned that results of JPHOTO given in the above table represent the maximum short circuit current obtainable if the back surface is perfect reflecting. If the back surface is perfect transmitting, i.e. one-pass, then JSC(max) < JPHOTO.

2.2 Results on Back Surface Field

The effect of back surface field (BSF) on the solar cell performance is analyzed in this section. Different diffusion profiles would give different amount of back surface fields. Its effect on solar cell performance is also analyzed.

The cell structures used here are the P+/N and the P+/N/N+ types whose impurity concentration profiles are given by

(1) P+/N Cell

$$N_{AA} - N_{DD} = C_0\exp[-(Z/L_1)^2] - C_B \tag{2.4}$$

(2) P+/N/N+ Cell-2

$$N_{AA} - N_{DD} = C_0\exp[-(Z/L_1)^2] - C_B - C_L\exp[-(L-Z)^2/L_2^2] \tag{2.5}$$

(3) P+/N/N+ Cell-6

$$N_{AA} - N_{DD} = C_0\exp[-(Z/L_1)^2] - C_B - C_L\exp[-(L-Z)^6/L_6^6] \tag{2.6}$$

Here, $C_0=1.25\text{x}10^{20}$, $C_B=5.0\text{x}10^{14}$ and $C_L=2.5\text{x}10^{20}$. The gold recombination model is used with a spatially constant gold concentration of $N_{TT}=4.465\text{x}10^{10}$ Au/cm^3 to give a midbase open circuit steady-state lifetime of 700 μs in the P+/N/N+ cell. This gold density is determined from the steady-state lifetimes versus position of a trial computer run in which the gold concentration was assumed to be $1.0\text{x}10^{10}$ Au/cm^3. The midbase steady-state lifetimes at the open circuit condition for the P+/N/N+ Cell-2 are $\tau_n=718.996$ and $\tau_p=718.987$ μs at the gold concentration of $4.4654\text{x}10^{10}$ Au/cm^3. These values are sufficiently close to the reported experimental values, 700 μs, so that a second iteration was not made.

A very important condition used in this calculation is that both the front and the back surfaces are short-circuited. The short-circuit boundary condition corresponds to infinite surface recombination rate or velocity. In addition, the surfaces are assumed to be neutral, that is, the interface recombination centers at the two surfaces are assumed to be at the neutral charge condition. This neutrality condition corresponds to a band of high density of interface states whose neutral Fermi level coincides with the silicon Fermi level at the silicon surface. Subsequent calculations, using a more concrete interface recombination center model, have confirmed the correctness of the present short circuit boundary condition. These calculations also showed that interface recombination had very small effect on the solar cell performance. This is an important result in view of the considerable current research efforts on the improvement of solar cell performance by reduction of interface or surface recombination velocity. Our calculations show that interface recombination cannot play a significant role because of the large retarding electric field from the diffusion profile of the diffused emitter and BSF layers.

2.2.1 Effect of Back Surface Field

The substantial improvement of the open circuit voltage from the presence of a back surface field in a solar cell was first recognized and analyzed in detail by Godlewski, Baraona and Brandhorst (GBB).[16] Their understanding and analyses were so complete that there is little need to further verify the presence of this effect. However, their analytical solutions assumed constant impurity concentrations at the two sides of the high-low junction barrier. Such an abrupt change of impurity concentration gives the upper limit of improvement one can expect from a back surface field layer. In practice, the concentration change in the diffused BSF layer is more spread out than the abrupt H/L transition assumed by GBB. If the concentration change is very gradual, spreading out over many diffusion lengths, then the improvement would not be as large. The calculations of this and the next section will show that the improvement is indeed very large and there is little difference between the two impurity diffusion profiles assumed.

The numerical calculations were made using the Trapezoid integration rule for the double integral of the distributed photocurrent generator before the improvement was made using the Simpson rule and the exact integration. They were not repeated using the improvement since the differences are small and the results are adequate for the study of the effects from BSF.

The solar cell characteristics with and without BSF using the Gaussian impurity profiles given by Equations (2.4) and (2.5) are compared in the following table.

Table 2.9 Effect of Back Surface Field on Silicon Solar Cell Performance at One AM1 Sun and 297K.

Computer Run No.	Cell Type	Impurity Profiles		EFF %	VOC mV	JSC mA/cm^2	FF
		Emitter	BSF				
RUN555	P+/N	$\exp(-X^2)$	none	16.236	554.11	32.456	.8028
RUN335	P+/N/N+	$\exp(-X^2)$	$\exp(-X^2)$	19.587	672.32	33.954	.7629

The P+/N/N+ BSF cell, given by RUN335, shows much higher EFF and VOC but only slightly higher JSC than the P+/N cell, given by RUN555. The improvement of VOC is large, amounting to 118 mV or almost 4.6(kT/q). This is 21% over the P+/N cell which has no BSF. JSC is increased only by about 1.5 mA/cm^2 or about 4.6% with the BSF. The fill factor, FF, actually decreased from 0.8028 to 0.7629 which reflects the presence of high injection level condition in the base of the BSF cell given by RUN335. The high injection level condition in the base also increases the steady-state base lifetime from 562 μs for the P+/N cell to 719 μs for the P+/N/N+ cell which accounts for the slight increase of JSC just noted. The high injection level condition may be further analyzed by noting that VOC and FF are directly related if the JSC vs VOC dependence is known. For the low injection condition, $J_{SC}=J_L\exp(qV_{OC}/kT)$, while for the high injection condition, $J_{SC}=J_H\exp(qV_{OC}/2kT)$.[17] Thus, for these ideal diode laws, the fill factor, FF, can be computed for a given V_{OC}. These are tabulated below for the two cells of Table 2.9 and compared with the exact values given there.

Table 2.10 Comparison of Exact and Ideal Theoretical Fill Factors.

Computer Run No.	Cell Type	VOC mV	FILL FACTORS		
			Exact	L.L.	H.L.
RUN555	P+/N	554.11	.8028	.818	.707
RUN335	P+/N/N+	672.32	.7629	.842	.742

The results of the P+/N cell given by RUN555 show that the exact FF (0.8028) is closer to the ideal low level FF (0.818) than the ideal high level FF (0.707). However, a detailed examination of the position variation of the electron and hole concentration inside the P+/N cell at the SC, MP (maximum power) and OC conditions indicates that the midbase values of the minority carrier or hole density in the n-base are 1×10^{13}, 2×10^{13} and 2×10^{14} while the equilibrium electron density is 5×10^{14} cm^{-3}. Thus, high level condition begins to set in under the open circuit condition in the P+/N cell at one AM1 sun but not at the short circuit or maximum power conditions.

For the P+/N/N+ cell of Run 335, the exact FF (0.7629) is closer to the ideal high level FF (0.742) than the ideal low level FF (0.842). The BSF high-low junction has nearly completely shielded the infinite surface recombination rate at the back surface. This can also be verified by using the analytical solutions obtained by Godlewski, Baraona and Brandhorst[16] in the limit of infinite back surface recombination velocity and much larger areal donor density in the N+ BSF layer than the N- base layer. In this case, the diode current-voltage characteristics can be approximated by

$$J_{SC} = (qn_iW_B/\tau_B)\exp(qV_{OC}/2kT) \qquad (2.7)$$

Using W_B=300 μm, $n_i=10^{10}$ cm^{-3}, τ_B=700 μs and J_{SC}=34 mA/cm^2, then the computed open circuit voltage is

$$V_{OC} = (2kT/q)\log_e[J_{SC}\tau_B/qn_iW_B] = (2kT/q)\log_e(5\text{x}10^5) = 678\ \text{mV}. \qquad (2.8)$$

This compares favorably with the exact numerical value of 672.32 mV. The good agreement shows that indeed the low-high (L/H) potential barrier of the N/N+ BSF junction is essentially a perfect reflecting barrier which shields the back surface recombination loss completely.

2.2.2 Effect of Diffusion Profile

It was just demonstrated that back surface recombination is almost completely shielded by the presence of the BSF of a Gaussian diffusion profile. Thus, a more abrupt diffusion profile with higher BSF would not be expected to further improve the shielding effect of the L/H or N/N+ potential barrier. A comparison of the analytical solution of (2.8) with the exact solution of Table 2.10 shows that only about 678-672.32=5.7 mV additional improvement can be expected from a larger potential barrier or steeper impurity gradient in the BSF layer. This anticipation is demonstrated by comparing the results of the Gaussian profile in Tables 2.9 and 2.10 with that of the measured phosphorus profile, $\exp(-X^6)$, which is steeper than the Gaussian profile, $\exp(-X^2)$. The net impurity concentration for the steeper BSF cell is given by Equation (2.6). The computed characteristics of the solar cells with these two BSF profiles are compared in the table given below.

Table 2.11 Effect of Diffusion Profile of the Back Surface Field Layer on Silicon Solar Cell Performance at One AM1 Sun.

Computer Run No.	Cell Type	Impurity Profiles		EFF %	VOC mV	JSC mA/cm^2	FF
		Emitter	BSF				
RUN335	P+/N/N+	$\exp(-X^2)$	$\exp(-X^2)$	19.587	672.32	33.954	.7629
RUN568	P+/N/N+	$\exp(-X^2)$	$\exp(-X^6)$	19.592	673.64	33.954	.7616

The results are as expected. J_{SC} is not changed and V_{OC} is increased by 1.32 mV in the more abrupt measured BSF diffusion profile. The small increase of V_{OC} indicates that the ideal Gaussian profile gives about the same solar cell performance as the measured phosphorus diffusion profile. The same conclusion may also be made for the measured boron diffusion profile which is in between the ideal Gaussian profile and the measured phosphorus profile.

2.3 Results on Interband Auger Recombination

Interband Auger recombination of electrons and holes can be an important recombination mechanism in regions of high carrier concentration because its steady-state recombination rate is proportional to the square of the majority carrier concentration and the steady-state lifetime is inversely proportional to the square of the majority carrier concentration. They are given by

$$R_{Auger} = c^nN^2P + c^pP^2N \qquad (2.9)$$

$$\simeq c^nN^2P \qquad \text{(n-Si)} \qquad (2.9n)$$

$$\simeq c^pP^2N \qquad \text{(p-Si)} \qquad (2.9p)$$

$$\tau_{Auger} = 1/[c^nN^2 + 2(c^n+c^p)PN + c^pP^2] \qquad (2.10)$$

$$\simeq 1/c^nN^2 \qquad \text{(n-Si)} \qquad (2.10n)$$

$$\simeq 1/c^pP^2 \qquad \text{(p-Si)} \qquad (2.10p)$$

Here, c^n is the interband Auger recombination rate of electron-hole pairs in which the energy is carried away by an electron and c^p is the rate in which the energy is carried away by a hole. The steady-state recombination rate and lifetime given above reduce to the simplified forms shown in Equations (2.9n), (2.9p), (2.10n) and (2.10p) in extrinsic material when the majority carrier concentration is much higher than the minority carrier concentration. For example, in p-Si, the electron lifetime [Equation (2.10p)] could be dominated by the interband Auger recombination mechanism if the hole concentration, P, is very high or the resistivity is very low. Values in Table 2.4 show that at 10^{18} carriers/cm^3, $\tau_p(\text{n-Si}) \simeq 2.6$ μs and $\tau_n(\text{p-Si}) \simeq 10$ μs. Thus, interband Auger recombination in the base can be the mechanism limiting the ultimate performance of silicon solar cell in low resistivity cells if all other recombination losses are eliminated.

It has also been thought that interband Auger recombination is important inside the diffused emitter and BSF layers as well as on their surfaces because of the very high majority carrier concentrations in these layers. This is not the case unless the majority carrier concentration is greater than about 10^{20} carriers/cm^3 over the entire layer because the diffusion lengths at 10^{19} carriers/cm^3 ($L_p \approx 2\mu m$ and $L_n \approx 6\mu m$) are much larger than the physical thickness of these layers (about 0.25 to 1 μm). However, interband Auger recombination could be important at the surface of the emitter and the BSF layers where the carrier concentration is greater than 10^{20} carriers/cm^3, provided the surface layer is sufficiently thick to give high enough Auger recombination current. Whether Auger recombination at the surface is important also depends on the magnitude of recombination at the interface or surface states. In our computer model, we have assumed an infinite interface recombination rate or velocity. Thus, the additional Auger recombination at the surface could not affect the results.

Because the interband Auger recombination rate is strongly dependent on the majority carrier concentration, we would expect it to be more important in the diffused emitter and BSF layers if the impurity diffusion profiles are very flat with high concentrations and drop abruptly at the junctions. The measured diffusion profiles of phosphorus and boron are indeed more abrupt than the ideal or standard Gaussian profile. Thus, it is useful to determine if such an abrupt and high concentration profile can significantly increase the interband Auger recombination current in the emitter and the BSF layers. For this study, we have varied the diffusion profiles to include the more abrupt measured diffusion profiles. The results are described below which confirm the initial expectation that the interband Auger recombination mechanism in the emitter and the BSF layers are not important, even if the interband Auger capture rates, given in Table 2.4, are in error and too low by as much as 100.

2.3.1 Emitter Layer

In order to separate the effect of Auger recombination in the emitter from that in the BSF layer, we shall first describe the results on cells with no BSF layer. P+/N cells are used in this study but the conclusion is equally applicable to the N+/P cells since the measured phosphorus and boron diffusion profiles have similar abruptness and the Auger recombination rates of electrons and holes (Table 2.4) are similar in magnitude. The two p-type emitter diffusion profiles used are the Gaussian and the measured profiles given by

$$N_{AA} - N_{DD} = C_0 \exp[-(Z/L_1)^2] - C_B \qquad (2.11)$$

$$N_{AA} - N_{DD} = C_0 [1 - (Z/L_1)^{2/3}] U(L_1 - Z) - C_B \qquad (2.12)$$

where $C_0 = 1.25 \times 10^{10}$, $C_B = 5.0 \times 10^{14}$, $U(z)$ is the unit step function and L_1 is determined by the junction depth of 0.25 µm. The gold recombination model is again used with a spatially constant concentration of $N_{TT} = 4.465 \times 10^{10}$ Au/cm^3 to give approximately 700µs base lifetime. The Auger recombination rates used are the latest and supposedly most reliable data which are given in Table 2.4.

Again the Trapezoid integration rule was used in these calculations and the results would not be significantly different if the more accurate Simpson rule for dλ and exact for dx are used in the double integral of the distributed photogenerators. Four computer runs are made for the two diffusion profiles with and without interband Auger recombination. The results are given below.

Table 2.12 Effect of Interband Auger Recombination in the Emitter on Silicon Solar Cell Performance at One AM1 Sun

Computer Run No.	Cell Type	Emitter Profile	Auger Recomb.	EFF %	VOC mV	JSC mA/cm^2	FF
RUN555	P+/N	$\exp(-X^2)$	NO	16.236	554.11	32.456	.80275
RUN556	P+/N	$\exp(-X^2)$	YES	16.226	554.09	32.438	.80275
RUN566	P+/N	$1-X^{2/3}$	NO	16.238	554.11	32.458	.80280
RUN567	P+/N	$1-X^{2/3}$	YES	16.198	554.03	32.382	.80279

As expected, interband Auger recombination in the diffused emitter has a larger effect in the measured emitter profile than the Gaussian profile. (i) It reduces the open circuit voltage by 0.02 mV in the Gaussian profile (RUN555 and RUN556) and 0.08 mV in the measured boron profile (RUN 566 and RUN567) out of 554.1 mV. (ii) It reduces the short circuit current more than the open circuit voltage, but still only by a small amount: 0.018 mA/cm^2 in the Gaussian profile and 0.076 mA/cm^2 in the measured boron profile out of 32.4 mA/cm^2. Thus, interband Auger recombination in the diffused emitter has negligible effect.

2.3.2 Back Surface Field Layer

Interband Auger recombination in the BSF layer will reduce the open circuit voltage. The L/H junction barrier is less effective in shielding out Auger recombination, which is closer to the L/H junction position, than the interface recombination at the back surface which is further away from the junction. However, numerical results tabulated below again shows that the reduction of VOC due to interband Auger recombination in the BSF layer is very small even for the measured phosphorus diffusion which is more abrupt than the ideal Gaussian profile. Six computer runs are given below. The results

Table 2.13 Auger Recombination in the Back Surface Field Layer on Silicon Solar Cell Performance at One AM1 Sun

Computer Run No.	Impurity Profiles		Auger Recomb	EFF %	VOC mV	JSC mA/cm^2	FF
	Emitter	BSF					
RUN568	$\exp(-X^2)$	$\exp(-X^6)$	NO	19.592	673.64	33.954	.76164
RUN570	$\exp(-X^2)$	$\exp(-X^6)$	YES	19.565	669.72	33.935	.76548
RUN569	$1-X^{2/3}$	$\exp(-X^6)$	NO	19.592	673.64	33.954	.76164
RUN571	$1-X^{2/3}$	$\exp(-X^6)$	YES	19.527	669.40	33.877	.76566
RUN335	$\exp(-X^2)$	$\exp(-X^2)$	NO	19.587	672.32	33.954	.76294
RUN500	$\exp(-X^2)$	$\exp(-X^2)$	YES	19.565	669.62	33.936	.76557

show that interband Auger recombination in the BSF layer decreases the open circuit voltage by about 4 mV for the measured phosphorus impurity profile and 2.7 mV for the Gaussian profile. It also shows that there is very small difference in V_{OC} between the Gaussian and the measured phosphorus diffusion profiles. The AM1 efficiency is changed by less than 0.06%.

2.4 Results on Surface Recombination

The exact numerical solution just described in section 2.3 showed that interband Auger recombination in the emitter and BSF layers has negligble effect on the AM1 performance of silicon solar cells. Since the results are based on exact numerical solution of a model with infinite surface or interface recombination velocity at the interface states, the influence of surface recombination was not explored. Although exact numerical solutions have been obtained which included finite interface recombination rate, the multitude of parameters make the exact solutions complicated to analyze. To make the results more transparant physically, a simple model will be used for which simple analytical solutions can be obtained. This simple model introduces an important physical parameter, the effective recombination velocity of a layer. It is the recombination velocity which will produce the same current as that at the recombination center in the bulk of the layer. This model will be used to assess the importance of surface recombination at the interface states on the silicon surfaces of a solar cell.

2.4.1 Emitter Surface Recombination

The simple model to be used has a constant majority carrier concentration in the emitter and hence constant Auger recombination lifetime. Interface recombination is characterized by a constant surface recombination velocity, S_I. The boundary condition for a P+ emitter is then given by

$$J_N(x=0) = qS_I[N(0) - N_E] = - qD_p[dN(x)/dx]_{x=0} \qquad (2.13)$$

This surface boundary condition at the emitter surface can be used to get a solution of the minoirty carrier (electron) diffusion equation in the p-type emitter:

$$dJ_N/dx = qD_n d^2N/dx^2 = R_{Auger} = c^P P^2 N = N/\tau_{Auger} \tag{2.14}$$

where the low level condition is assumed since the emitter has such a high majority carrier or hole concentration, P. The solution is given by the ideal Shockley diode equation with a modified saturation current:

$$J = J_0[\exp(qV/kT) - 1] \tag{2.15}$$

where the saturation current, J_0, is given by

$$J_0 = qN_ES_E \tag{2.16}$$

and S_E is the effective recombination velocity defined by

$$S_E = (D_E/L_E)\,\frac{(L_E/D_E)S_I + \tanh(W_E/L_E)}{1 + (L_E/D_E)S_I\tanh(W_E/L_E)} \tag{2.17}$$

D_E is the minority carrier (electron) diffusivity, D_n, in the emitter. L_E is the minority carrier (electron) diffusion length, $\sqrt{D_n\tau_n}$, where τ_n is the Auger lifetime given by Equation (2.10p). W_E is the thickness of the emitter layer.

The saturation current, expressed in terms of the effective recombination velocity given above, is particularly useful to determine the effect of interface recombination. A sketch of the solutions of this effective recombination velocity is given below where S_E is normalized to the diffusion velocity,

$v_{DF}=D_E/W_E$: $\mathcal{S}_E = S_E/v_{DF} = S_E/(D_E/W_E)$. (2.18)

There are four characteristic velocities in this general problem:

(i) $v_{R\infty} = D_E/L_E$	Recombination Velocity, thick emitter	$(W_E >> L_E)$	
(ii) $v_{R0} = D_EW_E/L_E = W_E/\tau_E$	Recombination Velocity, thin emitter	$(W_E << L_E)$	(2.19)
(iii) $v_{DF} = D_E/W_E$	Diffusion Velocity, thin emitter	$(W_E << L_E)$	
(iv) S_I	Interface Recombination Velocity		

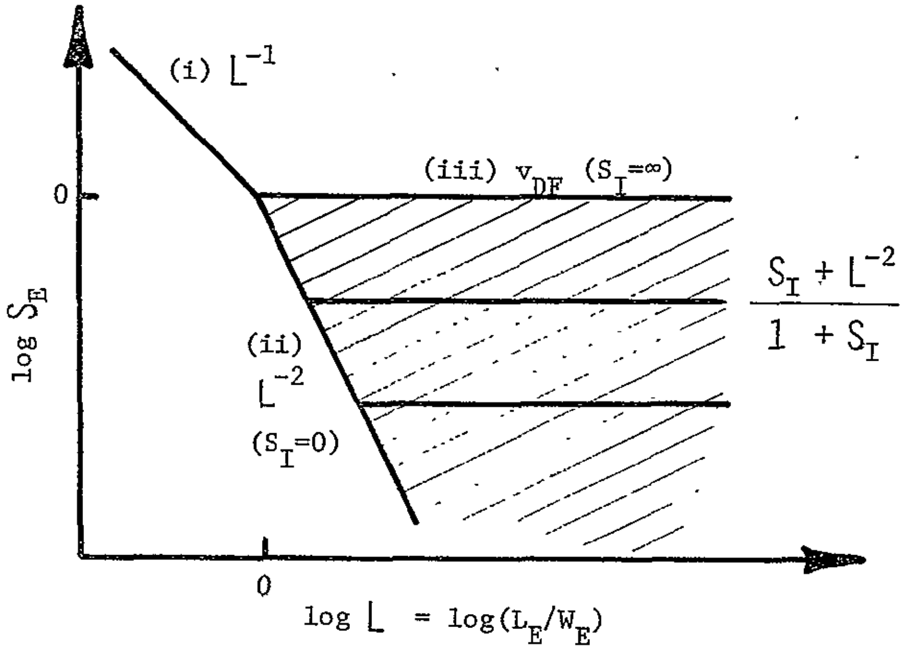

Figure 2.1 The effective recombination velocity of emitter recombination current as a function of minority carrier diffusion length with surface recombination velocity as the constant parameter.

The three asymptotic lines in the above figure, labled by (i), (ii) and (iii), correspond to the three characteristic velocities. When the emitter is thin compared with the minority carrier diffusion length, the effective recombination velocity will depend on the surface recombination velocity at the interface. This is in the shaded region in the above figure and it is given by

$$\mathcal{S}_E = (\mathcal{S}_I + \mathcal{L}^{-2})/(1 + \mathcal{S}_I) \qquad \text{or}$$

$$s_E = [s_I + (L_E^2/D_E W_E)]/[1 + (s_I W_E/D_E)]. \qquad (2.20)$$

Here, $\mathcal{S}_I = s_I/v_{DF} = s_I/(D_E/W_E)$. When the emitter becomes very thin, $\mathcal{L} = L_E/W_E \to \infty$, the effective recombination velocity approaches

$$\mathcal{S}_E = \mathcal{S}_I/(1 + \mathcal{S}_I) \qquad \text{or}$$

$$s_E = s_I/[1 + (s_I W_E/D_E)]. \qquad (2.21)$$

Numerical values are computed for the three characteristic velocities as well as the corresponding saturation currents for both n-type and p-type emitter of a thickness of W_E=0.25μm. Three constant majority carrier concentrations in the emitter are assumed. The numerical results are given in Table 2.14.

Consider the results for thin emitters which are items labeled (ii) and (iii) in the table, corresponding to the two asymptotic lines with the same labels in the figure on the preceding page. It is evident that the effective recombination velocity and the saturation current for the case of zero interface recombination, S_I=0, labeled (ii) are very small, giving unrealistically high open circuit voltages.

As the surface recombination velocity at the interface increases, the saturation current also increases and the open circuit voltage decreases. For the limiting case of infinite interface recombination velocity, the open circuit voltages are given by the line labeled (iii) in Table 2.14. The value for the p-type emitter (585 mV at 10^{18} holes/cm^3 and 666 mV at 10^{19} holes/cm^3) can be compared with the experimental value of the high efficiency Sandia P+/N/N+ cell[4]. Since the actual cell does not have a constant hole concentration as we have assumed in the simple model, a comparison is made based on the total hole concentration in the emitter, Q_{P+} which is about $20\text{x}10^{13}$ q/cm^2 given in the table. This is midway between our two cases of 10^{18} holes/cm^3 and 10^{19} holes/cm^3. A theoretical V_{OC} can be computed for the Sandia cell by using an average hole concentration, computed from the experimental Q_{P+}, which is $P_{AVE}=Q_{P+}/qW_E=8\text{x}10^{18}$ holes/cm^3. The electron diffusivity at this acceptor concentration is 3.5cm^2/s which gives a diffusion velocity of $v_{DF}=D_n/W_E$=140Kcm/s. The saturation current is $2.8\text{x}10^{-13}$A/cm^2 and the computed open circuit voltage is then V_{OC}=(kT/q)x log(0.03/$2.8\text{x}10^{-13}$)=656mV. Experimental value is 620mV and the difference is attributed to recombination in the base layer and in the BSF layer since

Table 2.14 Effects of Surface Recombination on the Interband Auger Recombination Current in Thin Emitter

P_P or N_N	(Carriers/cm^3)		10^{18}	10^{19}	10^{20}
W_E	(μm)		0.25	0.25	0.25
Q_E	(10^{13}q/cm^2)		2.5	25	250
D_n	(cm^2/sec)		7.1	3.0	2.2
τ_n	(sec)		10	100ns	1ns
L_n	(μm)		90	5.8	0.5
(i) $v_{R\infty}$	(cm/sec)		800	5K	44K
(ii) v_{R0}	(cm/sec)		2.5	250	25K
(iii) v_{DF}	(cm/sec)		284K	120K	88K
(i) $J_{R\infty}$	(10^{-14}A/cm^2)	(Thick)	1.3	0.8	0.7
(ii) J_{R0} $(S_I=0)$	(10^{-14}A/cm^2)	(Thin)	0.0035	0.035	0.35
(iii) J_{DF} $(S_I=\infty)$	(10^{-14}A/cm^2)	(Thin)	450	19	1.4
(i) V_{OC}	(mV)	(Thick)	736	748	752
(ii) V_{OC} $(S_I=0)$	(mV)	(Thin)	889	829	770
(iii) V_{OC} $(S_I=\infty)$	(mV)	(Thin)	585	666	734
Q_{P+}(Exp)	(10^{13} q/cm^2)			20	
V_{OC}(Exp)	(mV) (P+/N/N+)			620	
D_p	(cm^2/sec)		2.4	1.4	1.1
τ_p	(sec)		2.6μs	26ns	0.26ns
L_p	(μm)		25	1.9	0.17
(i) $v_{R\infty}$	(cm/sec)		960	7.4K	65K
(ii) v_{R0}	(cm/sec)		9.6	960	96K
(iii) v_{DF}	(cm/sec)		96K	56K	44K
(i) $J_{R\infty}$	(10^{-14}A/cm^2)	(Thick)	1.5	1.2	1.0
(ii) J_{R0} $(S_I=0)$	(10^{-14}A/cm^2)	(Thin)	0.015	0.15	1.5
(iii) J_{DF} $(S_I=\infty)$	(10^{-14}A/cm)	(Thin)	150	9.0	0.7
(i) V_{OC}	(mV)	(Thick)	732	738	742
(ii) V_{OC} $(S_I=0)$	(mV)	(Thin)	851	792	732
(iii) V_{OC} $(S_I=\infty)$	(mV)	(Thin)	613	686	752

maximum emitter recombination has been assumed in this sample calculation.

Another useful result from Table 2.14 is that it provides an estimate of the range of interface recombination velocity within which significant effect can be expected. For example, consider the 10^{19} p-type emitter whose data are given in the upper half of Table 2.14. The diffusion velocity, line (iii), is 120,000 cm/sec. Thus, the interface recombination velocity, S_I, must be significantly smaller than this value to reduce the recombination current. On the other hand, there is no use to reduce the interface recombination velcoity to a value below 250 cm/sec, which is the effective recombination velocity due to interband Auger recombination in the emitter, v_{RO}.

The simple model allows us to make a simple and rapid estimate of the importance of interband Auger recombination in the emitter and at what interface recombination velocity does interface recombination become important. The parameters that determine the relative importance are the minority carrier diffusion velocity, $v_{DF} = D_E/W_E$, and the effective interband Auger recombination velocity in the entire emitter, $v_{RO} = D_E W_E / L_E^2 = W_E/\tau_E$. This effective recombination velocity in the entire emitter not only applies to the Auger recombination mechanisms but also the Shockley-Read-Hall thermal recombination mechanism as well as other localized recombination mechanisms as long as a constant recombination lifetime can be defined. As another illustration, if the emitter recombination lifetime from all mechanisms is 1 ns (similar to the third column of Table 2.14), then the effective emitter recombination velocity is $v_{RO}=W_E/\tau_E=0.25\text{x}10^{-4}/10^{-9}=25\text{K}$ cm/sec. Thus, it would be futile to decrease the surface recombination velocity at the interface to less than 25K cm/sec.

These numerical results also show that the conclusion will not be altered unless the interband Auger capture rates are in error and too small by 100.

2.4.2 Back Surface Field Recombination

The relative importance of recombination in the bulk of the back surface field layer and at the interface states on the back surface can be estimated using the simple model of constant majority carrier concentration employed in the emitter in the preceding section. The analytical solutions of Godlewski[16] can be used for the interband Auger recombination mechanism in the BSF layer since it has a constant recombination lifetime when we assume a constant majority carrier concentration in this layer.

The conclusion obtained from the analytical solution is very similar to that just obtained for the emitter region:- for a total electron concentration in the back surface field layer, Q_{BSF}, of less than about 10^{15} q/cm^2 and an average electron or majority carrier concentration of less than about 10^{19} $carriers/cm^3$, Auger recombination cannot be very important. The relative importance of Auger or other recombination mechanisms in the BSF layer to the surface recombination at the interface states on the back surface is determined in the same way as that in the emitter which was just described in section 2.4.3. Thus, the interface recombination velocity on the back surface must fall below the diffusion velocity but above the effective recombination velocity of the entire BSF layer in order to have any influence on the open circuit voltage.

2.5 Results on Enhanced Impurity Solubility

The diffused emitter and back surface field layers are frequently used to getter the recombination impurity centers in the bulk of silicon devices because of the enhanced solid solubility in these high concentration layers from impurity-shallow donor or impurity-shallow acceptor interactions at the diffusion temperatures. In solar cell and other shallow emitter structures, the back surface field layer is a particularly effective getter since it is formed by high temperature diffusion for a sufficiently long time to allow the recombination impurities in the bulk to outdiffuse into this layer. One common practice is to form the N+ BSF layer at a high temperature to getter out all the metallic recombination impurities in the bulk of silicon.

Gettering by the BSF or diffused emitter layer will improve the base lifetime but at the same time will reduce the emitter and the BSF lifetimes. If the emitter or the BSF layer has a high concentration of the recombination impurities from gettering action, the short circuit current and the open circuit voltage will suffer. The magnitude of this degradation can be predicted by the computer model and is the subject of this section.

In the following two subsections, we shall describe the results of enhanced solubility of the recombination impurity in the emitter of a P+/N cell and in the back surface field layer of a P+/N/N+ cell. The two-level gold recombination model will be used. The solubility of gold is assumed to be proportional to the concentration of the boron or phosphorus impurity in the diffused layer.[18] A constant background gold concentration of 4.465×10^{10} Au/cm^3 is also assumed to be present in the entire sample in order to simulate the experimental OC base lifetime of 700 μs at one AM1 sun reported for the Sandia high-efficiency cells.[4]

The difference between this study and that reported in TR-1 is as follows. In TR-1, the gold concentration in the base was raised in the same proportion as that in the diffused emitter or BSF layer. In this report, the gold concentration in the base is kept constant while it is increased in the emitter and the BSF layers. The constant gold concentration in the base is a better model for the effects of gettering and enhanced solubility of recombination impurity centers in the emitter and the BSF layers. The gold concentration in both this and previous reports is assumed to be proportional to the diffusion impurity concentration. Other possible dependences are $N_{Au} \propto N_{DD}^2$ or N_{DD}^3, etc. and $N_{Au} \propto N_{AA}^2$ or N_{AA}^3, etc. depending on the detailed impurity pairing and complexing mechanisms involved. These stronger dependences will decrease the lifetime in the emitter or BSF layer near the junction further and hence increase the recombination current even more than the linear dependences, $N_{Au} \propto N_{DD}$ and $N_{Au} \propto N_{AA}$. The computer results of this section show already very substantial reduction of solar cell performance from the linear dependences.

2.5.1 Emitter Layer

The principal effect to be expected from an enhanced solubility of gold in the diffused emitter is a reduction of the short circuit current because of the high absorption of the photons in the emitter layer. Reduction of the open circuit voltage should be smaller than that of the short circuit current since VOC is mainly determined by base recombination and BSF in this high resistivity cell. The first series of study was made to determine the effect of emitter impurity diffusion profile since a steeper or more abrupt profile would give a higher gold solubility and hence shorter lifetime closer to the emitter junction. This would increase the emitter recombination current. The second series of study was made to determine the amount of performance degradation as a function of increasing gold solubility in the emitter. These are summarized in the following tables.

The effect of the emitter impurity profile is studied using the standard Gaussian profile, $\exp(-X^2)$, and the measured boron profile, $1-X^{2/3}$. The cell characteristics are tabulated below.

Table 2.15 Effect of Emitter Diffusion Profile on Enhanced Solubility of Recombination Center and Silicon P+/N Solar Cell Performance at One AM1 Sun

Computer Run No.	Emitter Profile	%Au In Emitter	EFF %	VOC mV	JSC mA/cm^2	FF
RUN556	$\exp(-X^2)$	0	16.226	554.09	32.438	.80275
RUN567	$1 - X^{2/3}$	0	16.198	554.03	32.382	.80279
RUN564	$\exp(-X^2)$	1	15.788	552.75	31.643	.80268
RUN563	$1 - X^{2/3}$	1	14.951	551.34	30.053	.80237
RUN565	$\exp(-X^2)$	10	15.027	548.17	30.362	.80282
RUN560	$1 - X^{2/3}$	10	14.176	548.50	28.658	.80194

From the results of the table, we note two important trends. First, the enhanced solubility of gold in the emitter can significantly reduce the short circuit current but has little effect on the open circuit voltage. Second, the diffusion profile also has a significant reduction effect on the short circuit current and little effect on the open circuit voltage. The more abrupt drop-off of the measured boron profile, $1 - X^{2/3}$, gives a higher gold concentration and lower electron lifetime near the emitter junction than the Gaussian profile, $\exp(-X^2)$. For example, the short circuit current decreases from 32.438 mA/cm^2 (RUN556) for the Gaussian emitter impurity profile without solubility enhancement to 28.658 mA/cm^2 (RUN560) for the measured boron profile with a gold solubility equal to 10% of the boron concentration. This is a drop of 3.780 mA/cm^2 or nearly 12% in JSC due to enhanced solubility of recombination center in the emitter. The drop of JSC accounts for the decrease of efficiency from 16.226% to 14.176% since the open circuit voltage and the fill-factor both decrease only slightly: ΔVOC=-5.59mV=-1.0% and ΔFF=-0.00081=-0.10%.

The results of these examples show that a 2% decrease of AM1 efficiency may occur, from 16 to 14%, if the recombination center solubility in the emitter is enhanced to a value of 10% of the emitter impurity concentration. Such a high value is not unreasonable since impurity interaction can make the recombination center equal to dopant concentration under favorable conditions. Although the sample calculation is made for a boron diffused emitter of a P+/N silicon solar cell, the same kind of performance degradation would be expected in a N+/P cell due to a similar behavior of enhanced solubility of the recombination centers in the N^+ diffused emitter.

A more detailed calculation has been made on the performance degradation as a function of the gold solubility in the diffused emitter in a P+/N silicon solar cell using the measured boron diffusion profile, $1-X^{2/3}$. A residue gold concentration of 4.564×10^{10} Au/cm^3 is again assumed. Auger recombination is included but its effect is negligible. The results are tabulated below.

Table 2.16 Effect of Enhanced Solubility of Recombination Center in the Diffused Emitter on the Performance of Silicon P+/N Solar Cells at One AM1 Sun

Computer Run No.	% Au In Emitter	EFF %	VOC mV	JSC mA/cm^2	FF
RUN567	0	16.198	554.03	32.382	.80279
RUN559	.00893	16.169	553.98	32.328	.80278
RUN563	1.0	14.951	551.34	30.053	.80237
RUN562	5.0	14.347	549.47	28.946	.80209
RUN560	10.0	14.176	548.50	28.658	.80194
RUN561	20.0	14.030	547.08	28.440	.80181

An additional result over the previous table is illustrated in this table. It shows that performance degradation tends to slow down as the gold solubility increases above the 5 to 10% range. This may be used to simulate the operating life of a cell as affected by the diffusion of metallic impurities into the emitter from the contact electrodes. The above table suggests that there could be a significant initial rapid drop of the JSC due to diffusion of the contact metal into the diffused emitter but subsequent changes of JSC would be both small and slow as suggested by the saturation trend in Table 2.16 when gold concentration in the emitter is increased.

In practice, it has been generally observed that a N+ layer with a high concentration of phosphorus is an excellent getter for metallic recombination impurities at high temperatures while a similarly strong gettering action has not been observed unambiguously in high concentration boron layers. Thus, the results just obtained for the enhanced solubility of gold in the emitter is probably more applicable to phosphorus diffused emitter of a N+/P or a N+/P/P+ silicon solar cell. To avoid performance degradation due to enhanced solubility of metallic recombination impurities in the diffused emitter, one would prefer an arsenic emitter which is probably not as good a getter as phosphorus for a N+/P cell or a boron emitter which is likely to be a poor getter compared with phosphorus for a P+/N cell.

The above quantitative result of enhanced solubility of metallic impurity in the emitter with enhanced emitter recombination is consistent with some experimental observations on the Westinghouse silicon cells and on the high efficiency Sandia silicon cells. In the Westinghouse experiments, it has been observed that the Ti-doped P+/N cells have higher efficiency than the Ti-doped N+/P cells. Similarly, higher efficiency seems to have been obtained in the P+/N/N+ cells than in the N+/P/P+ cells in the Sandia high efficiency cell experiments. Base recombination may also be different in these cases which may account for the difference between the N+/P and the P+/N cells but the results of the emitter recombination enhancement due to enhanced solubility in the N^+ layer are not contradictory to these experimental results. In the Westinghouse cells doped with the highest Ti concentration, there is an indication that enhancement of Ti solubility in the phosphorus emitter may account for a large part of the efficiency and short circuit current degradation. This is described in sections 3.2 and 3.3.

2.5.2 Back Surface Field Layer

Enhanced solubility of recombination impurity in the high concentration diffused back surface field layer would reduce the open circuit voltage because of the increased recombination rate and current in the back surface field layer. It would have little effect on the short circuit current which is mainly affected by recombination near the front surface of the cell. The results of computer calculation using the Simpson $d\lambda$ and exact dx integration rules for the distributed photocurrent generators are tabulated in the following table. Again, a constant background gold concentration of $4.465\text{x}10^{10}$ Au/cm^3 is assumed in the entire cell. The gold concentration is enhanced in the BSF layer and the enhancement is assumed to be a constant percentage of the phosphorus impurity concentration. Auger recombination is not included in this computation but its effect was demonstrated to be negligibly small in section 2.3. The measured boron and phosphorus diffusion profiles are used in the calculation. The net ionized impurity concentration using Table 2.5 is given by

$$\begin{aligned} N_{AA}(Z) - N_{DD}(Z) = {} & 1.25\text{x}10^{20}[1 - (Z/L_1)^{2/3}]U(L_1-Z) \\ & - 5.0\text{x}10^{14} \\ & - 2.5\text{x}10^{20}\exp[-(L-Z)^6/L_2^6] \quad \text{Ions/cm}^3 \qquad (2.22) \end{aligned}$$

The results of seven computation runs for increasing gold solubility in the BSF layer are tabulated below. They show a significant reduction of the open circuit voltage when the gold concentration in the diffused BSF layer is only 1% of the phosphorus concentration. In fact, the values obtained in RUN576 are very close to the values of the experimental high efficiency cells.[4]

Table 2.17 Effect of Enhanced Solubility of Recombination Center in the Back Surface Field Layer on the Silicon P+/N/N+ Solar Cell Performance at One AM1 Sun

Computer Run No.	% Au in the BSF Layer	EFF %	VOC mV	JSC mA/cm^2	FF
RUN577	0.0	19.261	672.86	33.421	.76162
RUN576	1.0	18.784	627.82	33.373	.79718
RUN578	5.0	18.125	602.17	33.242	.80511
RUN579	10.0	17.730	591.01	33.114	.80557
RUN580	20.0	17.279	580.16	32.913	.80462
RUN581	50.0	16.620	566.26	32.502	.80296
RUN582	P+/N/∞	15.991	553.68	31.989	.80282

The enhanced solubility of recombination impurities in the BSF layer can also be used to model the degradation of operating life due to diffusion of metallic impurities from the back contact metal into the BSF layer. From the results of RUN577, which has no gold in the BSF layer, and RUN576, which has 1% gold in the BSF layer, it is evident that a large degradation of the open circuit voltage can be expected in a short time during the initial operation of the cell. Subsequent reduction is considerably smaller for the same amount of increase of gold concentration. In the limit when the BSF layer is completely saturated with a very high concentration of recombination impurities, the performance of the P+/N/N+ cell is degraded to that of a P+/N cell (RUN582 on the last line of Table 2.17) if the recombination impurities do not penetrate significantly into the base region of the cell. For thick cells, such as the 300 μm assumed, deep penetration into the quasineutral base layer is probably rather slow compared with the penetration through the 1 μm thick BSF layer.

2.6 Defect-Impurity Recombination Centers

If all of the metallic impurity recombination centers can be eliminated, then the ultimate efficiency of a silicon solar cell would be determined by the remaining deep level recombination centers formed by physical lattice defects such as silicon vacancies and interstitials; defect complexes such as the divacancies and higher vacancy clusters; defect-impurity complexes such as the oxygen-vacancy pair or A-center, the phosphorus-vacancy pair or the E-center, and a boron-vacancy complex yet to be positively identified; shallow-level doping or junction forming impurities, such as a phosphorus or boron pair or clusters; and diffusion-induced strain and dislocations. These imperfections can be generated in the diffused emitter and BSF layers by the high concentrations of diffusion impurities (boron and phosphorus) which form the emitter and BSF layers.

The computer studies made in this section are aimed to determine the silicon solar cell performance limitations imposed by recombination at these residual imperfection centers in the diffused emitter and BSF layers. These studies are undertaken using two recombination models to simulate recombination in the emitter and BSF layers separately. The recombination parameters of these recombination models were tabulated in Table 2.2 and 2.3. The basis for selecting these parameters are described in the following subsections.

(A) Emitter Recombination Model

For the diffused emitter layer, the divacancy or boron-vacancy center is used as the recombination model. A single level donor-like recombination center is assumed whose concentration is given by

$$N_{TT}(Z) = (\mathrm{FRAC})\times 1.25\times 10^{20}[1 - (Z/L_1)^{2/3}]U(L_1-Z) + N_{TTB} \qquad \text{Centers/cm}^3 \qquad (2.23)$$

The factor, FRAC, is the fraction of the boron in the diffused emitter which has formed the recombination complex. N_{TTB} is the residual recombination density in the entire cell. It covers the range of 0 to 10^{11} Centers/cm^3 and is assumed to be spatially constant. The background recombination density can be converted into a steady-state base lifetime which can be used as a universal or recombination-species-independent parameter under some restricted conditions.[1]

The boron-defect complex has neither been positively identified nor characterized. However, transient capacitance measurements on one MeV irradiated N+/P silicon diodes have indicated a strong donor recombination level at E_V+354 mV in the lower half of silicon energy gap.[19] This level was also shown to be the main contributor to the leakage current under reverse bias.[20] Thus, it will be used as the recombination model in the boron diffused emitter. The recombination parameters of this donor level are listed in Table 2.2 and it will be referred to as the boron vacancy complex, B_xV_y, although it may involve an unknown impurity.

The recombination coefficients listed in Table 2.2 are obtained as follows. e_{p-1} is first computed from the experimental transient capacitance data and e_{n0} is first computed from the experimental leakage current data. Experimental accuracy was two to three significant figures. More significant figures are listed to insure that mass action law holds numerically. c_{n-1} and c_{p0} are estimated from the pre-exponential factor of the thermal emission rates, e_{n0} and e_{p-1}, assuming an Arrhenius relationship of the form $AT^2\exp(-\Delta E/kT)$. The emission rates are then recomputed so that the mass action law at equilibrium (dark and zero applied voltage), $e^t_{n0}e^t_{p-1}/c^t_{n-1}c^t_{p0}=n_i^2$ is satisfied. The large ratio, c^t_{n-1}/c^t_{p0} = 64.3, is consistent with the donor-like charge state of this center. Although values of these parameters given in the above table may not be accurate, the solar cell results obtained here can also be stated in terms of the electron and hole steady-state lifetimes in the base and emitter instead of the concentration of the donor recombination center. Thus, the results of this study on the solar cell performance will not be significantly changed when accurate recombination rates become available since it is necessary only to add a scale factor to the recombination level density.

(B) BSF Recombination Model

The existence of the phosphorus-vacancy or E-center in the diffused BSF layer is probably more certain than that of the boron-vacancy complex in the diffused emitter. The PV pair has been positively identified by many experiments on phosphorus-doped silicon. To study the effect of the PV or E center on the silicon solar cell performance, the following position variation of the concentration of the PV recombination center is assumed.

$$N_{TT}(Z) = N_{TTB} + (FRAC)x2.5x10^{20}\exp[-(L-Z)^6/L_2^6] \quad \text{Centers/cm}^3 \qquad (2.24)$$

A constant background, denoted by N_{TTB} is assumed to simulate the base lifetime observed experimentally. The factor, FRAC, is the fraction of the phosphorus atoms in the diffused BSF layer which have formed the PV pair. Detailed theoretical analysis of experimental phosphorus diffusion profiles have suggested a concentration of PV pair with a value of FRAC=0.6 for certain diffusion conditions.[2] In this study, FRAC will be varied from 0 to 0.8 to simulate a wider range of possible conditions.

From transient capacitance data, the following recombination parameters were obtained for the PV center and are used in this study.[19] The thermal emission rate of trapped electrons, e_{n1}, comes from the experimental data. The thermal capture rate, c_{n0}, is computed from the pre-exponential factor of the thermal emission rate data using $AT^2\exp(-\Delta E/kT)$. c_{p1} is estimated by assuming a hole capture radius of 25A at the negatively charged phosphorus-vacancy pair, giving $c^t_{p1}=\sigma^t_{p1}\Theta_p=\pi r_p^2\Theta_p=\pi(25x10^{-8})^2x10^7\approx 2x10^{-6}$ cm^3/sec. Such a large capture radius is acceptable in view of the large physical size of a pair (it occupies two lattice sites) and the long range Coulomb force associated with the negatively charged acceptor state of the PV center. The thermal emission rate of trapped hole, e^t_{p0}, is then computed from the mass action law, $e^t_{p0} = n_i^2 c^t_{n0} c^t_{p1} / e^t_{n1}$. The parameters are tabulated in Table 2.3.

Note that the ratio of the capture rates for the PV center is about $c^t_{p1}/c^t_{n0} = 7.3$ compared with the corresponding ratio, $c^t_{n-1}/c^t_{p0} = 64.3$, for the boron-vacancy-impurity complex listed in Table 2.2. This difference gives another variation for checking the sensitivity of the results on the recombination model parameters used in the calculation.

2.6.1 Emitter Layer

The effect of recombination at the boron-vacancy center (B_xV_y where x may be zero) in the emitter layer is more complicated than that at the phosphorus-vacancy center in the back surface field layer. This complication arises because emitter recombination can affect both J_{SC} and V_{OC} while recombination in the BSF layer reduces mainly V_{OC} and has little effect on J_{SC}.

The reduction of V_{OC} with increasing emitter recombination is large if emitter recombination dominates over base recombination. The amount of reduction of J_{SC} with increasing emitter recombination, however, is not affected by base recombination, but increasing base recombination will further reduce J_{SC}.

A family of curves is computed to show the effect of emitter recombination on the efficiency at one AM1 sun in silicon P+/N/N+ cells. These curves are given in Figure 2.2 where the efficiency is plotted as a function of the boron-vacancy complex density, represented by the factor FRAC in Equation (2.23), in the boron diffused emitter. FRAC = 1.0 would give a recombination center density of $N_{TT}=1.25\text{x}10^{20}$ centers/cm^3 at the front surface. On the x-axis, values of two other parameters are also given. These are the open circuit minority carrier (hole) lifetime and diffusion length. Since they both vary with position, their values at 0.2μm from the front surface or 0.05μm from the P+/N junction are given.

The density of the base recombination center, simulated by the B_xV_y center, is the constant parameter in these curves, with values of $N_{TT}(\text{base})=10^{10}$ (curve 10) to 10^{13} (curve 13) centers/cm^3. Reference curves for negligible base recombination are also given which are labeled 1 and 1A. Interband Auger recombination is not included except in curve 1A since its effect is small as indicated by curve 1A compared with curve 1. The steady-state minority carrier base

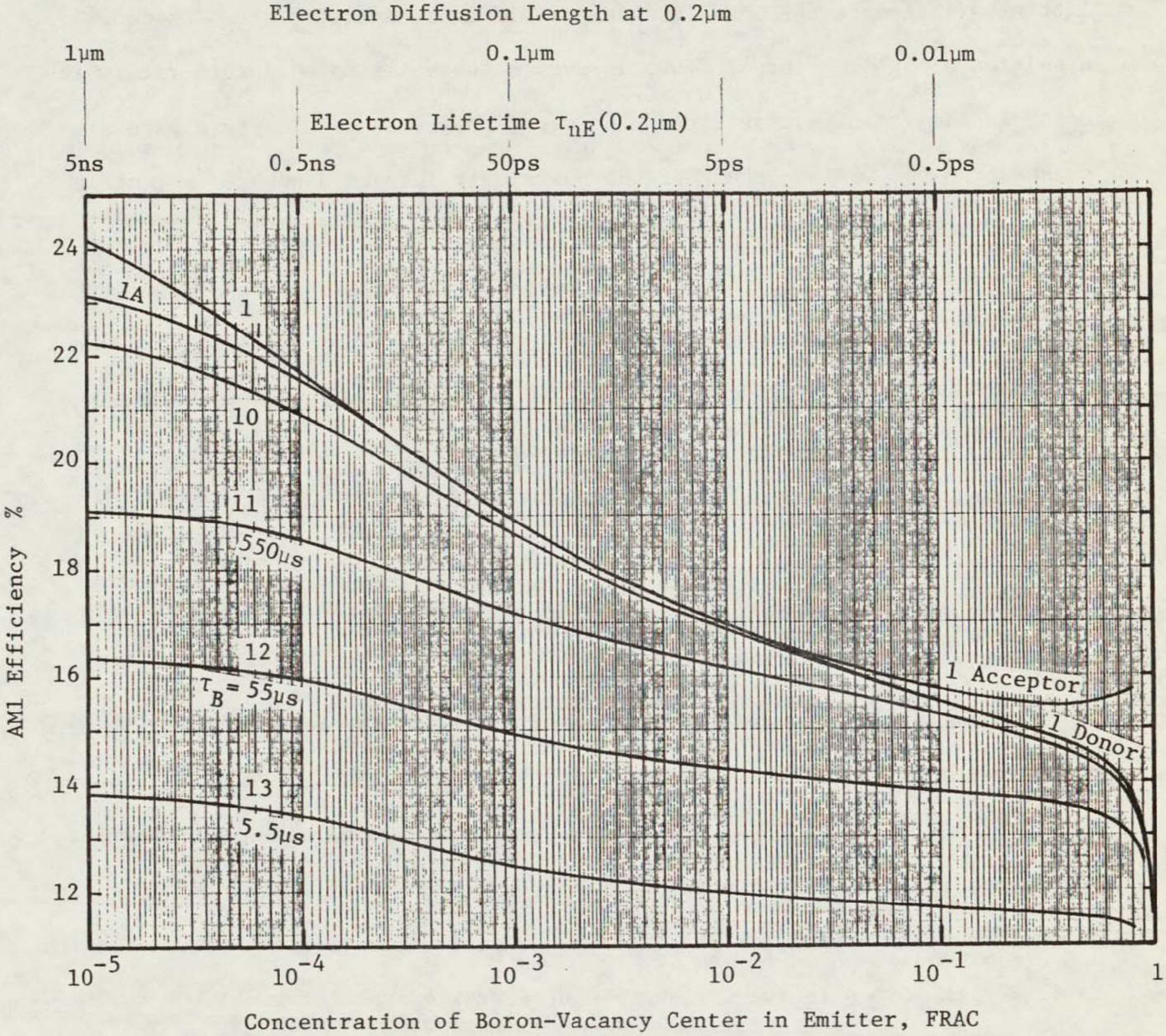

Figure 2.2 AM1 efficiency as a function of boron-vacancy defect recombination center concentration and emitter diffusion length and lifetime in P+/N/N+ silicon solar cells with the base recombination center density as the constant parameter.

lifetimes are shown next to each curve, ranging from 5.5μs to 550μs. There is little variation of the base lifetime at different emitter recombination densities along each curve. This is due to the small hole capture rate which controls the recombination rate. The much larger electron capture rate arises from the Coulomb force of the positively charged donor recombination center which gives a ratio of c_{n-1}/c_{p0} = 64.3 from Table 2.2.

The effect of emitter recombination on the efficiency can be examined by considering the EFF vs FRAC curve of low base recombination, such as curve 11 which has a base lifetime of 550μs. It is evident that a substantial decrease of the efficiency occurs only when the emitter lifetime of electrons at the edge of the junction space charge layer becomes substantially smaller then 1 ns. A 4% decrease, from 19% to 15%, would occur if the emitter recombination center density is 10% (FRAC=0.1) of the boron concentration in the emitter.

For higher base recombination, such as curves 12 and 13 with 55μs and 5.5μs base lifetimes, the effect of emitter recombination is reduced by about 2 or a efficiency drop of only about 2%. When base recombination is important, increasing emitter recombination will decrease mainly the short circuit current which results in efficiency degradation. This is illustrated in the following table for the 5.5μs (curve 13) and 550μs(curve 11) base lifetimes.

Table 2.18 Effect of the Donor Recombination Center in the Diffused Emitter on Silicon P+/N/N+ Solar Cell Performance at One AM1 Sun.

logNTTB=	11	13	11	13	11	13	11	13
FRAC	EFF(%)		VOC(mV)		JSC(mA/cm^2)		FF	
10^{-5}	19.086	13.807	659.58	516.85	33.420	30.042	.76993	.79066
10^{-4}	18.543	13.415	651.97	516.05	32.617	29.239	.77536	.79062
10^{-3}	17.184	12.456	633.07	513.94	30.646	27.264	.78759	.79047
10^{-2}	16.174	11.927	607.30	512.38	29.587	26.203	.80043	.78993
10^{-1}	15.232	11.668	577.17	510.33	29.153	25.767	.80497	.78898
0.8	13.633	11.271	526.30	498.76	28.933	25.547	.80287	.78661

Consider first the short circuit current, J_{SC}. It is evident that the decrease of J_{SC} due to increasing emitter recombination is about 4.5 mA/cm^2 (33.420-28.933=4.49 for $N_{TTB}=10^{11}$ and 30.042-25.547=4.50 for $N_{TTB}=10^{13}$). The decrease is relatively independent of base lifetime or base recombination which is increased by a factor of 100 between these two curves.

Next, consider the open circuit voltage, V_{OC}. Column 13 of V_{OC} in Table 2.18 shows that if base recombination dominates over emitter recombination, then an increase of emitter recombination from FRAC=10^{-5} to 0.8 only decreases VOC by 516.85-498.76=18.1mV. However, if base recombination is small or negligible (column 11 of V_{OC} in the table), then V_{OC} is significantly reduced by increasing emitter recombination. In this example, the reduction is 659.58-526.30=133mV or about 5kT/q.

Two additional effects are illustrated in this calculation, one is the ultimate efficiency imposed by interband Auger recombination in the emitter and the other is the effect of an acceptor recombination center in the p-type emitter instead of the donor just studied. Their effects on efficiency are demonstrated in Figure 2.2.

Interband Auger recombination in the emitter will slightly lower the efficiency when the emitter impurity recombination center density is negligible. This is illustrated by curves 1 and 1A in Figure 2.2. Curve 1 has no interband Auger recombination while curve 1A has. Both curves have a very low base recombination rate (10 centers/cm^3) in order to emphasize the effect of interband Auger recombination in the emitter. It is evident that the difference between curve 1 and 1A at a FRAC(emitter)=10^{-5} is only about 1%. This would be much less than 1% if higher and more realistic base recombination is assumed, such as 10^{11} of curve 11. In the limit of zero emitter impurity recombination, emitter Auger recombination would reduce the efficiency by 25.548-23.484=2.06%. These are maximum values of curves 1 and 1A as FRAC → 0 in Figure 2.2.

The difference between a compensating (donor-like) and noncompensating (acceptor-like) recombination center in the boron diffused emitter on the efficiency is illustrated by the two curves labeled 1-acceptor and 1-donor in Figure 2.2. There is negligible difference at low concentration or low FRAC of these centers. However, when FRAC approaches 1, a donor recombination center will compensate the charge of the diffused boron acceptor impurity in the emitter, thereby reducing the hole density in the emitter and the P+/N barrier height. This will reduce the open circuit voltage which is directly related to the equilibrium potential barrier height of the P+/N junction but will not affect the short circuit current. The solar cell characteristics due to the charge difference of these two recombination centers in the emitter are given in Table 2.19 for the case of FRAC=0.8. The numerical result furhter illustrates that VOC is greatly reduced by compensation over that of non-compensation while JSC does not change.

Tabel 2.19 Effect of the Charge States of the Recombination Center in the Emitter on Silicon P+/N/N+ Solar Cell Performance at One AM1 Sun. FRAC=0.8.

Computer Run No.	Recombin. Center	EFF %	VOC mV	JSC mA/cm^2	FF
RUN613	Acceptor	15.659	589.62	29.101	.81338
RUN622	Donor	13.752	527.62	29.083	.79689

2.6.2 Back Surface Field Layer

The effect of recombination at the phosphorus-vacancy (PV) center in the back surface field layer is to reduce the open circuit voltage from a high value determined by base recombination or by surface recombination at the contact to the value of an equivalent P+/N/∞ or P+/N cell with no BSF and with infinite surface recombination rate. This was already demonstrated in section 2.2.1 using the gold recombination model. The PV recombination center does not behave too differently.

A family of curves is again computed to illustrate the reduction of efficiency by recombination in the BSF layer and to show how this reduction is affected by base recombination. This is given in Figure 2.3. The AM1 efficiency at one sun is plotted as a function of the fraction (FRAC) of phosphorus which is converted into PV pair in the BSF layer. This FRAC is also translated into the minority carrier (hole) steady-state lifetime at a position 299.20μm which is 0.8μm from the back surface and 0.2μm from the N/N+ junction. The N/N+ junction is located at 1.0 μm from the back surface. Corresponding hole diffusion length at this location is also obtained. Both the hole lifetime and diffusion length are indicated on the FRAC or x-axis in Figure 2.3.

We first note that inclusion of interband Auger recombination in the BSF will only reduce the efficiency slightly as indicated by curves labeled 1 and 1A. 1A has Auger recombination. This is similar to earlier results. However, the compensation effect just described for the emitter layer does not appear in the BSF layer to any significant amount. This is due to the fact that as FRAC approaches 1, the large density of PV recombination center will already have reduced the N/N+ junction to a N/∞ junction so that compensation cannot reduce the effective back surface recombination velocity further. On

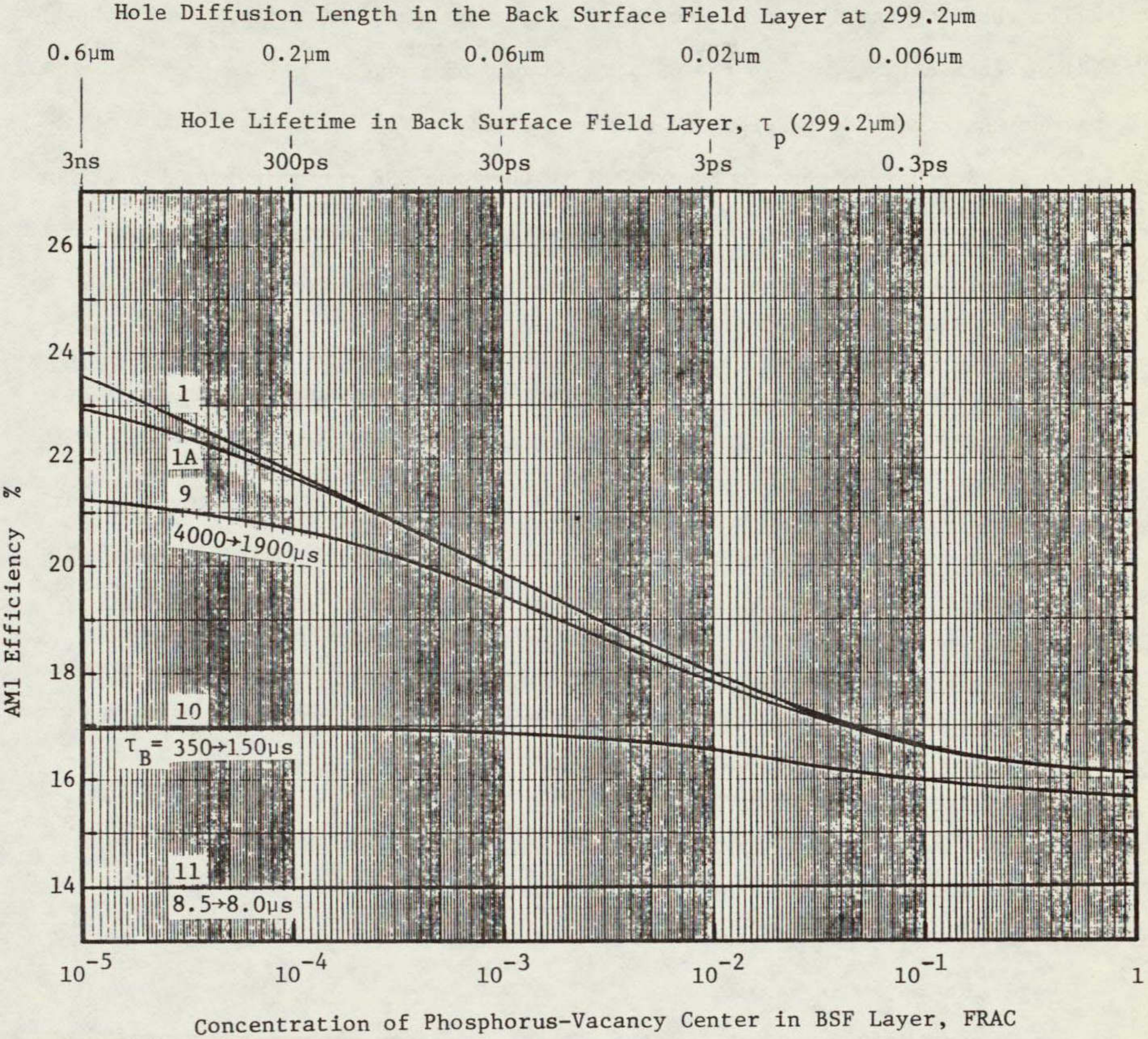

Figure 2.3 AM1 efficiency as a function of phosphorus-vacancy recombination center concentration, back surface field lifetime and diffusion length in P+/N/N+ silicon solar cells with the base recombination center density as the constant parameter.

the other hand, if the recombination center in the BSF layer is noncompensating, then the N/N+ barrier height would not be reduced as FRAC approaches 1. But the recombination rate in the BSF layer would increase to such a high value that the N/N+ barrier becomes essentially a N/∞ contact.

Another feature in Figure 2.3 is that the BSF recombination has almost no effect on the efficiency when the base lifetime of holes is below about 10μs which corresponds to a hole diffusion length of about 100μm. This is demonstrated in curve 11. For a hole lifetime in the base of 350μs, BSF recombination can reduce the efficiency at most by 1.5% as indicated by curve 10.

The large variation of the steady-state hole lifetime in the base with BSF recombination center density, for example from 350μs to 150μs in curve 10, comes from the intermediate injection level condition in the base. At low FRAC or low base recombination, the injection level is high so that the hole lifetime approaches the high level lifetime which is $\tau_{n0}+\tau_{p1}=361+50=411\mu s$ from Table 2.3 for $N_{TTB}=10^{10}$ centers/cm^3. As FRAC increases toward one, the BSF recombination also increases so that the injection level in the base decreases due to the lower hole concentration reaching the N/N+ high-low junction. This would decrease the hole lifetime toward the low injection level value which is $\tau_{p1}=50\mu s$.

The reduction of the efficiency with increasing BSF recombination or FRAC, indicated in Figure 2.3, arises mainly from a decrease of VOC just stated. This is further demonstrated by the numerical results tabulated in Table 2.20 for $N_{TTB}=10^{10}$ centers/cm^3.

Table 2.20 Effect of the PV Acceptor Recombination in the Back Surface Field Layer on Silicon P+/N/N+ Solar Cell Performance at One AM1 Sun.

Computer Run No.	FRAC	EFF %	VOC mV	JSC mA/cm^2	FF
RUN671	10^{-5}	16.958	638.27	32.650	.72359
RUN672	10^{-4}	16.946	632.01	32.646	.73035
RUN673	10^{-3}	16.860	611.98	32.619	.75099
RUN674	10^{-2}	16.542	583.27	32.461	.77810
RUN675	10^{-1}	15.973	560.12	32.037	.79151
RUN680	0.99	15.664	551.71	31.748	.79522

The tabulated results show that recombination in the BSF layer significantly reduces VOC, from 638.27 to 560.12 or 78.2mV, but the reduction of JSC is rather small, from 32.650 to 32.037 or 0.61mA/cm^2 when the PV recombination center density is increased to 10% of that of the phosphorus concentration in the diffused BSF layer. The last row for RUN680 demonstrates the absence of the performance dropoff when 99% of the phosphorus donors in the BSF layer are converted into phosphorus-vacancy acceptor recombination centers. This is in contrast to the large compensation effect by the boron-vacancy donor complex on the boron acceptor in the diffused emitter discussed in the preceding subsection and shown in Figure 2.2.

A useful guide can be deduced from the results in this table. The improvement of efficiency and VOC that can be achieved by reducing the PV recombination center in the BSF layer is not very large. Based on 95 mW/cm^2 AM1 incident power, efficiencies of 16.8%, with VOC=610mV and JSC=32.2mA/cm^2, have been obtained from Sandia's high efficiency cells.[4] Comparing these numbers with those in Table 2.20 suggests that the concentration of the electrically active PV centers which are also active recombination sites in the phosphorus diffused BSF layer cannot be higher than about 10^{-3} times the phosphorus concentration. This is substantially smaller than the value, FRAC=0.6, that is assumed in the detailed analysis of the phosphorus diffusion profile.[2] In order to bring these into agreement, the capture rates of electrons and holes at the PV center given in Table 2.3 must be reduced by 600. This would reduce the capture radius of holes by the negatively charged PV center from 25A assumed earlier to 1A. The value of 1A is inconsistent with the physical size of the PV center which must occupy two silicon lattice sites or about 5A. It is also inconsistent with the long range Coulomb force of the negatively charged PV pair. Alternatively, the active PV recombination center density may be indeed very low due to slow cooling and other annealing treatment after the 1000C phosphorus diffusion.

3. TECHNICAL DISCUSSION - Ti-DOPED CELLS

3.0 Objectives

Substantial efforts have been spent to study the effects of metallic impurities on the performance of silicon solar cells since they are not completely removed in solar cell grade silicon single crystals due to cost considerations. These studies were carried out by Westinghouse and previously by Monsanto groups. Recently, accurate minority carrier diffusion length and lifetime measurements in the base of solar cells made on impurity-doped silicon have been made by the Northrop group. The crucial parameters needed to characterize the recombination properties at these metallic impurities are the thermal capture and emission rates of electrons and holes. Alternatively, it is sufficient to completely characterize the recombination properties at an impurity recombination center by having three parameters: the thermal capture rates of electrons and holes and the thermal activation energy. But, these parameters are still not accurately determined. Measurements by the so-called DLTS (Deep Level Transient Spectroscopy) method have given qualitative indications of only the energy levels. Accurate values of these parameters can only be obtained by the *transient capacitance methods* which employ the following techniques:[17]

TSCAP - Thermal Stimulated Capacitance

VSCAP - Voltage Stimulated Capacitance

LSCAP - Light Stimulated Capacitance

These methods will provide all of the recombination parameters, including both the thermal emission rates, activation energies, and *the thermal capture rates at thermal equilibrium.*

Without these parameters, it is difficult to accurately predict the maximum allowable concentration of a metallic recombination impurity to give a prescribed solar cell performance. However, a number of experimental measurements have been made on Ti-doped silicon solar cells so that an extrapolation can be made to give a preliminary set of values for these recombination parameters at the Ti recombination centers. These measurements include the Ti concentration in each crystal, the minority carrier diffusion length in the base from which the minority carrier lifetime can be computed, the extrapolated minority carrier base lifetime using an experimental curve of open circuit voltage decay lifetime (τ_{OCD}) versus diffusion length lifetime (τ_B), the concentration of carbon and oxygen in the starting silicon crystal, and some preliminary but fairly reliable thermal emission rates and energies obtained by us in Ti-doped p-type Westinghouse silicon single crystals.

In this chapter, a study of the Ti on the silicon solar cell performance is undertaken using these preliminary recombination parameters. The study is aimed to provide an indication of the range of solar cell performance one can expect in the presence of Ti impurity. It also serves to indicate the type of projection that can be made from the computer model and the ambiguities which need to be resolved by the transient capacitance measurements.

3.1 Approach

The approach undertaken here is similar to that described in section 2.1 of the previous chapter for high efficiency cells. The same computer model will be used but the Ti recombination model will be used instead of the gold recombination model used previously. The details of the Ti recombination model will be described in subsection 3.1.1. The device and material parameters to be used are those from the processing data sheet of Westinghouse so that the computed solar cell performance characteristics can be compared with the experimental data given by Westinghouse. Since the experimental cells have no anti-reflection coating, the surface reflection loss at the silicon surface is included in the photogenerators of the model.

3.1.1 Ti Recombination Model

One electron and two hole thermal capture coefficients at the Ti centers in Ti-doped silicon are obtained from the base lifetime versus Ti concentration data. These data are shown in Figure 3.1. The Ti concentration data are taken from the Westinghouse Quarterly Reports[21] and the Monsanto Final Report.[22] The base lifetime data are taken from the Northrop Final Report [23] which were computed by them from their diffusion length measurements on cells made on the Ti-doped silicon of Monsanto and Westinghouse. For the more recent Westinghouse silicon doped with Ti which had no diffusion length measurements made by Northrop (crystal number greater than W056), the curve of τ_{OCD}(Westinghouse data) versus τ_{DL}(Northrop diffusion length data) given by Northrop is used to compute the base lifetime since τ_{OCD} for each cell is given by Westinghouse so that the base lifetime, τ_{DL}, can be read off the τ_{OCD} vs τ_{DL} curve. This procedure provides an estimated base lifetime for all of the more recent Westinghouse cells.

The points in Figure 3.1 can be separated into three groups. The lowest

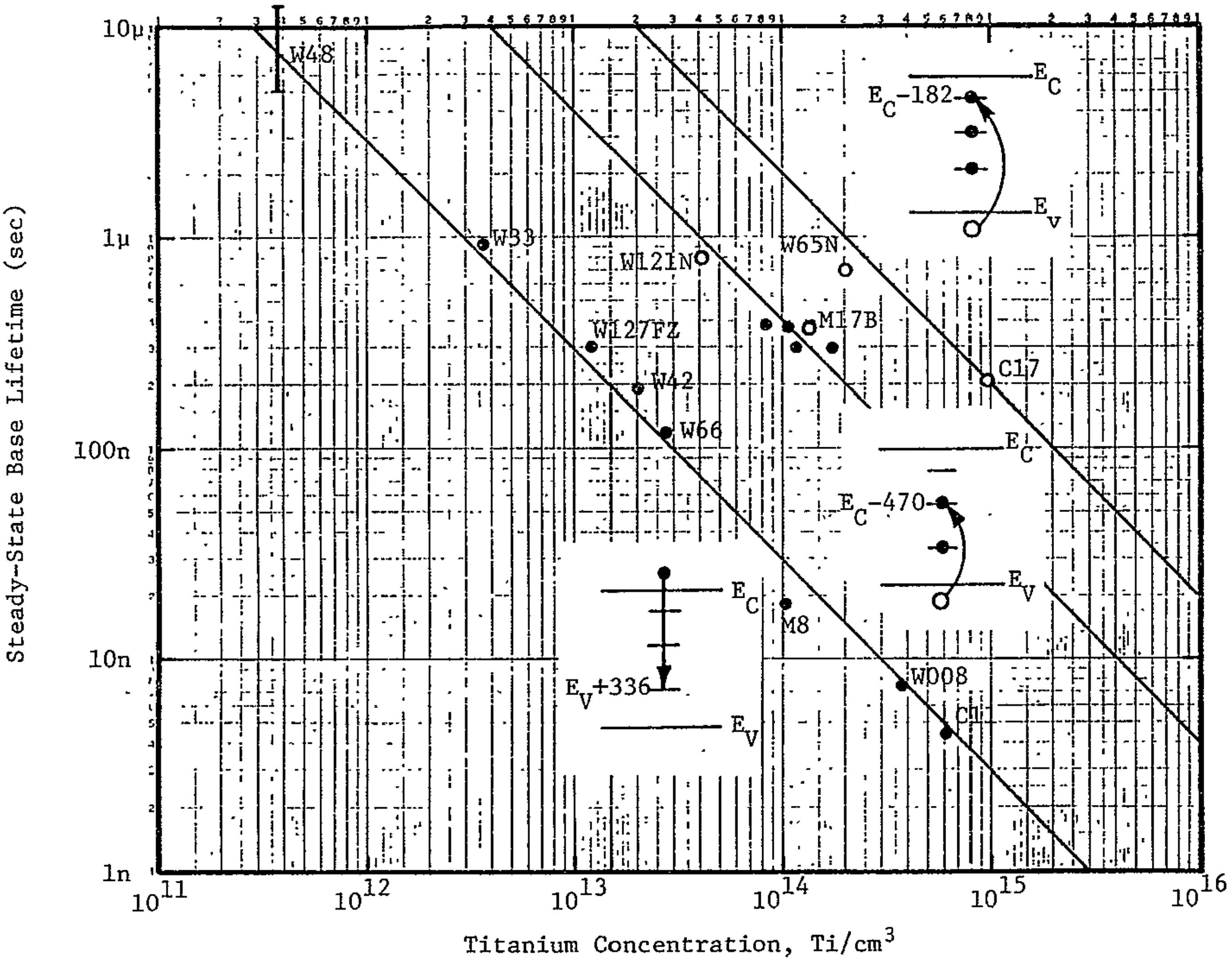

Figure 3.1 Base minority carrier lifetime as a function of Ti concentration. Insets show the corresponding electron or hole capture transitions.

line contains points from p-base silicon cells doped with Ti. The lifetimes correspond to electrons (minority carriers) captured into the E_V+336 mV level. This energy level and the other two at E_C-470 mV and E_C-182 mV were determined by VSCAP transient capacitance measurements on Ti-doped silicon using Mg/p-Si Schottky barrier diodes. The assignment of these τ_B-N_{Ti} data to this transition is consistent with the position of the bulk Fermi level in the p-type silicon which is E_F-E_V = 168→229 mV at 297K. Thus, the Fermi level position is below this Ti level which is located at E_T-E_V = 336 mV. Since the lifetime is small, it is also consistent to assume that these are low level lifetimes in the base. In addition, it is not inconsistent with some of the preliminary experimental indications of Westinghouse that emitter recombination is probably not too important even if the N+ phosphorus diffused emitter has some gettering action of Ti but this point must be more carefully investigated.

The middle and the highest lines on Figure 3.1 contain two points each from Ti-doped n-type silicon, one from Westinghouse and the other from Monsanto. Although there are two points each, they are unmistakenly separated even allowing the large uncertainty of the data which we have not shown in the figure. In addition, there are many points from p-type Ti-doped Westinghouse crystals which are clustered around the middle line. These are discussed later.

For the four points from n-type silicon, a distinction among them is that the two crystals on the middle line contain either a high concentration of carbon or a low concentration of oxygen, while the two crystals on the upper line have just the opposite proportional of carbon and oxygen. Their carbon and oxygen concentrations were given by Westinghouse[21] and Monsanto[22] and are given in Table 3.1 on the next page.

The basis for these two groupings to give the two upper lines in Figure 3.1 is as follows. The upper line for the two crystals, W065 and C17B,

Table 3.1 Carbon and Oxygen Concentration in n-Si Doped with Ti.

Crystal Number	Resistivity ohm-cms	Dopant 10^{15}P/cm^3	Titanium 10^{14}Ti/cm^3	Carbon 10^{16}C/cm^3	Oxygen 10^{16}O/cm^3
W065N	1.8	3.	2 or 3.5	<2	176
W121N	1.8	3.	0.4	4.7	121
C17B	0.6	10.	9.5	1.5	174
M17B	0.54	11.	<1.3	0.6	5.6

were grown by the Czochralski method and have high oxygen concentration (about $1.8\text{x}10^{18}$ O/cm^3). They also have low carbon concentration. On the other hand, for the two crystals on the middle line, crystal W121 has a relatively higher carbon concentration and somewhat lower oxygen concentration, while crystal M17B has low concentration of both oxygen and carbon. The following tentative model seems to emerge. The two high oxygen crystals with low carbon content, W65 and C17B, are likely to have a shallow acceptor level associated with the oxygen which is present. Such a shallow level, in the form of an oxygen-vacancy pair, is known to form when vacancies are generated in oxygen-rich silicon crystals. Vacancy is very mobile and gets trapped next to the oxygen. The high Ti concentration during crystal growth may creat a high density of vacancies which may be trapped at the oxygen sites upon cooling. This model is suggested by the well-known oxygen-vacancy energy level in silicon which is E_C-174 mV and it is nearly equal to observed activation energy of an acceptor level, E_C-182 mV, using the VSCAP method. Thus, this upper level and line can be attributed to the OV center but a more complex $O_xV_yTi_z$ center cannot be ruled out.

The association of the E_C-182 mV level with the OV pair or oxygen is also consistent with the two crystals lying on the middle line, W121 and M17B. The M17B crystal, grown by float-zone method, has a low concentration of both oxygen and carbon. Thus, the oxygen-vacancy acceptor will have very low concentration, if it exists in M17B. The hole lifetime in the n-type base cell of this crystal is then associated with the hole capture into the middle level, E_C-470 mV since the E_C-182 mV level has low concentration.

For the W121 crystal, the carbon concentration is high, although not substantially higher than the other three crystals. But the higher carbon concentration suggests that the OV level (E_C-182 mV) is impeded by the presence of carbon. For example, carbon may form a complex with the OV pair and either render it electrically inactive or drastically change its energy level. Thus, the hole capture transition is again dominated by the E_C-470 mV level in this crystal due to the lack of the E_C-182 mV level.

There are four Ti-doped p-Si from Westinghouse, W102, W122, W123 and W140, whose points are clustered around the middle line for the E_C-470 mV level. At least two possibilities exist to account for these points: (i) the E_V+336 mV level does not exist in these crystals and the transition involves electron capture into the E_C-470 mV level, and (ii) high level injection level occurs in the base of the cells from these crystals so that hole capture into the E_V+336 mV level dominates the recombination.

It is obvious that all of these considerations can be readily checked if transient capacitance measurements are made on these crystals.

The capture rates can be readily computed from the slope of the straight lines of Figure 3.1. The corresponding thermal emission rates for the majority carriers were obtained from VSCAP measurements. These results are listed in Table 3.2 on the next page and are used for further calculation to give the complete set of recombination parameters at thermal equilibrium.

The majority carrier capture rates can be estimated by assuming a temperature independent capture cross section and by assuming that the emission rates are independent of the electric field. Then, $e_n=c_nN_C\exp(-E/kT)$ and

Table 3.2 Experimental Thermal Emission and Capture Rates in Ti-Doped Silicon

$E_V + 336$ mV Level

$c_n = 3.7\times10^{-7}$ $\mathrm{cm^3/sec}$

$e_p = 1.1\times10^{11}(T/300)^2\exp(-336\mathrm{mV}/kT)$ 1 /sec

$E_C - 470$ mV Level

$e_n = 5.6\times10^{13}(T/300)^2\exp(-470\mathrm{mV}/kT)$ 1 /sec

$c_p = 2.5\times10^{-8}$ $\mathrm{cm^3/sec}$

$E_C - 182$ mV Level

$e_n = 3.6\times10^{11}(T/300)^2\exp(-182\mathrm{mV}/kT)$ 1 /sec

$c_p = 5.\ \times10^{-9}$ $\mathrm{cm^3/sec}$

$e_p=c_pN_V\exp(-E/kT)$. These can be used with the experimental emission data to compute the thermal capture rates, c_n and c_p. The fourth parameter, the minority carrier thermal capture rate, of each of the three levels is computed using the mass action law, $e_ne_p=c_nc_pn_i^2$, where three of the rates are already obtained and n_i is also given.

The solar cell calculations are made at 297K, The kinetic recombination coefficients computed using the procedure just described are obtained for the three levels observed in Ti-doped silicon solar cells. These are given in Table 3.3 on the next page.

The choice of the charge state shown in Table 3.3 is based on the relative size of the electron and hole capture rates and the position of the level to a band edge. The two lower levels are assumed to be donor like since $c_n >> c_p$ for both levels. The upper level is assumed to be acceptor like since it is closer to the conduction band edge and since the OV center is an acceptor.

Table 3.3 Derived Recombination Parameters of the Ti Related Energy Levels in Si at 297K. n_i=1.036x10^{11}/cm^3.

E_C-182 Acceptor Level				Lifetime at 10^{14} Levels/cm^3
c_n	=	.13 E-07	cm^3/sec	τ_n = 760 ns
e_n	=	.3 E+09	1 /sec	
c_p	=	.5 E-08	cm^3/sec	τ_p = 2000 ns
e_p	=	.22 E-04	1 /sec	
E_C-470 Donor Level				
c_n	=	.2 E-05	cm^3/sec	τ_n = 5 ns
e_n	=	.6 E+06	1 /sec	
c_p	=	.25 E-07	cm^3/sec	τ_p = 400 ns
e_p	=	.92 E+01	1/sec	
E_V+336 Donor Level				
c_n	=	.4 E-06	cm^3/sec	τ_n = 25 ns
e_n	=	.16 E+01	1 /sec	
c_p	=	.82 E-08	cm^3/sec	τ_p = 1150 ns
e_p	=	.22 E+06	1 /sec	

In the computer calculation, we shall use the two lower levels and assume that they are coupled and come from one species of Ti recombination centers. No experimental data are available to show if the two lower levels are associated with a single Ti recombination center or they are two independent energy levels associated with two different species of Ti recombination centers. For example, in the two independent level model, one of the two Ti species can be an isolated substitutional Ti center while the other, a Ti-O or Ti-A pair where A is an unknown impurity.

3.1.2 Computer Model

The computer model is nearly identical to that used for the high efficiency cell studied in chapter 2 and described in section 2.1.2. The only difference is that the length of the transmission line is 250 μm instead of 300 μm since the experimental Westinghouse cells have a nominal thickness of 250 μm. For the p-base cell, the emitter is 0.25 μm and for the n-base cell, the emitter is 0.185 μm. There is no BSF layer in either of these cells. However, the four region model is still used in which the fourth region, occupied by the BSF layer previously, is just an extension of the third region or the quasi-neutral base region. In projecting the maximum allowable Ti concentration for a desired efficiency, cells with BSF are used in the computer model since they give the best efficiency with the highest open circuit voltages. For these BSF cells, the four region model is needed and the BSF layer is assumed to be 1 μm thick while the fourth region is 2 μm thick.

The better integration scheme, exact for dx and Simpson for dλ, is used for all of the calculations made for Ti-doped cells.

3.1.3 Device and Material Parameters

The parameters in Table 3.4 are used so that results of this study can be compared with the experimental data of the Westinghouse Ti-doped cells. The parameter values are obtained from the Quarterly Reports of Westinghouse. The fabrication history as well as the electrical properties of the finished silicon solar cells doped with metal impurities are extremely well documented in these quarter reports.

Three columns are given in Table 3.4, one for the p-base cell, one for the n-base cell and the third for the highest efficiency Ti-doped P+/N/N+ cell. The separate listings of the experimental cells is due to the slight differences in the base dopant impurity concentration, surface concentration and profiles.

Table 3.4 Device and Material Parameters of Ti-Doped Silicon Solar Cells of Westinghouse.

Item	Parameter	p-Base	n-Base	P+/N/N+
1	T (K)	297	297	297
2	n_i (cm^{-3})	0.1036E+11	0.1036E+11	0.1036E+11
3	L (μm)	250	250	250
4	X_J (μm)	0.250	0.185	0.250
5	X_{BSF} (μm)	-	-	-
6	ρ_B (ohm-cm)	3.5 → 4.5	1.4 → 2.2	
7	C_0 (cm^{-3})	5.0E+20	2.5E+20	5.0E+20
8	C_B (cm^{-3})	5.0E+15	5.0E+15	5.0E+15
9	C_L (cm^{-3})	-	-	2.5E+20
10	Emitter Profile	1 - X (two)	$1 - X^{2/3}$	$1 - X^{2/3}$
11	BSF Profile	-	-	$\exp(-X^6)$
12	N_{TT} (Ti/cm^3)	constant 4E11 → 4E14	constant 4.0E+13	constant 4E11 → 4E14

For the phosphorus diffused emitter of the p-base cell, the diffusion profile was obtained by sheet resistance-anodic etching method.[8] It contains two linear segments due to the particular diffusion schedule and ambient gas used. This profile drops off slower than the $\exp(-X^6)$ profile used previously for the phosphorus diffused N+ layer. The boron diffused emitter profile was also obtained by sheet resistance-anodic etching method.[9] It is essentially identical to the $1-X^{2/3}$ profile used earlier for the high efficiency cell studies in chapter 2. Slight differences between these empirically fitted profiles and the experimental profiles will not significantly affect the final results and conclusions as we have demonstrated in the high efficiency cell studies in Chapter 2 if the enhancement of Ti solubility in the emitter is not large which is apparantly the case for low Ti concentrations. For high Ti concentrations (4×10^{14} Ti/cm^3), enhancement of solubility in the emitter may be large and the solar cell characteristics will be more critically dependent on the emitter diffusion profile.

3.1.4 Solar and Optical Properties

The AM1 solar spectra, silicon absorption coefficient, $\alpha(\lambda)$, and silicon surface reflection coefficient, $R(\lambda)$, used in this study are those given in Table 2.7 of section 2.1.4. To simulate the performance of the Westinghouse cells, silicon surface reflection loss is taken into account by reducing the incident solar spectral irradiance [the column $P(\lambda)$ in Table 2.7] by the factor $1-R(\lambda)$. This is done by including the factor $1-R(\lambda)$ in the integrand of the distributed photocurrent generator given by Equation (2.1).

The maximum AM1 photocurrent that can be collected in a 250 μm thick silicon solar cell with no anti-reflection coating is calculated to be 22.025 mA/cm^2. Without surface reflection loss, it is 34.198 mA/cm^2. Thus, the surface reflection loss at a bare silicon surface amounts to a reduction of $[1 - (22.025/34.198)] = 0.356$ or 36%. However, this reduction factor is not a constant since it will depend on the cell thickness as well as the distribution of the recombination centers within the cell because of the wave length dependence of the absorption and reflection coefficients. But, the figure of 0.36 or 36% can be used as a rule of thumb estimate when considering the short circuit current and the efficiency. An estimate of the increase of the open circuit voltage due to the higher photocurrent when there is no surface reflection loss can also be made. If we assume low level injection condition inside the cell, then

$$\Delta V_{OC} \approx (kT/q)\log_e(34.198/22.025) = 11.37 \text{ mV}$$

For high injection level, the increase from an uncoated to a perfectly coated cell would be twice this value or 22.75 mV.

3.2 Results on p-Base Cells

In order to compare the computed results with the experimental data of the Ti-doped silicon cells fabricated by Westinghouse, the diffusion profile and the dopant concentration are selected to match their reported data. From Table 3.4, the net ionized impurity concentration profile used in the computer program is given by

$$\begin{aligned} N_{DD} - N_{AA} &= 5\text{x}10^{20}[1.04 - 3.29(Z/L_1)] - 5\text{x}10^{15} & 0 < Z < 0.07694\mu\text{m} \\ &= 2\text{x}10^{19}[1.00 - 1.00(Z/L_1)] - 5\text{x}10^{15} & 0.07694 < Z < L_1 \\ &= -5\text{x}10^{15} & L_1 < Z < 250\mu\text{m} \qquad (3.1) \end{aligned}$$

Here, $L_1 = X_J/[1-25C_B/C_0] = 0.2500626156$ μm and the large number of significant figures given is to indicate that there is no jump in the $N_{DD}-N_{AA}$ value at the junction X_J, only a change in slope or concentration gradient. This impurity concentratiion profile fits the experimental profile obtained by Westinghouse for the phosphorus diffused emitter very well as demonstrated in Figure 3.2.

The Ti concentration is assumed spatially constant but as we shall see from the results, there is an indication of Ti pileup in the phosphorus diffused emitter for the highest Ti concentration cell from Westinghouse crystal W008.

The cells are not coated with anti-reflection coating, thus, the surface reflection loss is included in the calculation by the procedure described in section 3.1.4.

The computed results for the N+/P cells are compared with Westinghouse's experimental data.[21] Comparisons are made for EFF, VOC, JSC, and FF in Figure 3.3(a) to (d) as a function of Ti concentration. Data of only four Ti-doped N+/P cells are included which are from Westinghouse crystals W048, W033, W066 and W008, in increasing Ti concentration.

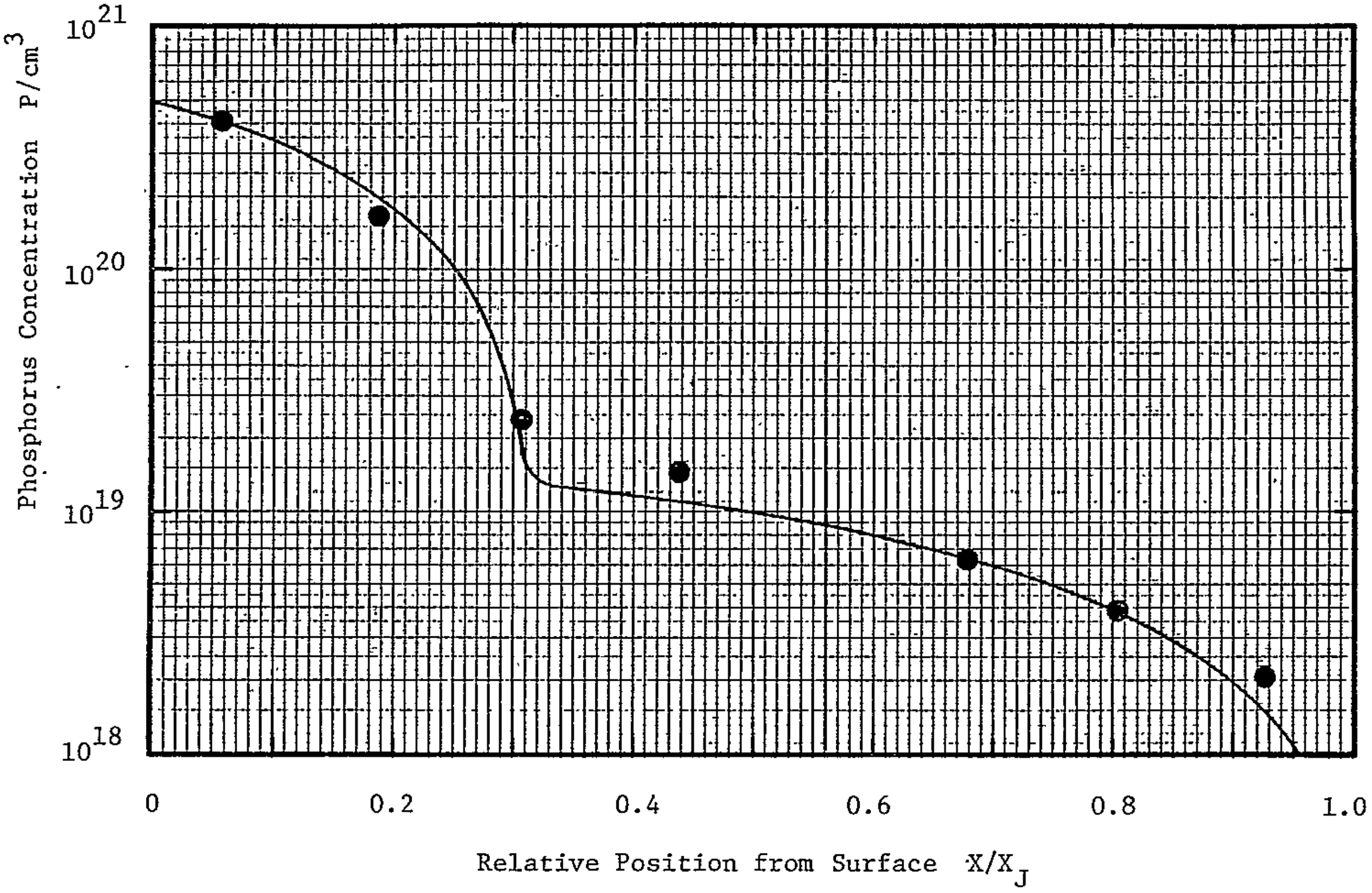

Figure 3.2 The phosphorus diffusion profile (experimental points) and the two constant concentration-gradient empirical fits (solid curve) to experiments. X_J=0.25μm.

The best experimental-theoretical agreement is obtained for the open circuit voltage, shown in Figure 3.3(b). This is probably due to its insensitivity to random experimental variations of device and material parameters since it is measured at zero current. The agreement also indicates self-consistency in the assumption that base recombination dominates in these Ti-doped cells.

The poorest agreement is in the fill-factor. This is probably due to its high sensitivity to the contact resistance at both the front and back surface contacts and also its dependences on the high conductance paths which may have a high occurrence rate in the emitter of cells highly doped with Ti.

The efficiency and the short circuit current show better theoretical-experimental agreement at low Ti concentrations as revealed in Figures 3.3(a) and (c). For the highest Ti concentration cells (crystal W008, $N_{TT}=3.8\times10^{14}$ Ti/cm^3), the experimental values are more than 50% below the theory, although VOC [Figures 3.3(b)] and FF [Figure 3.3(d)] are nearly equal to the theory. Thus, the smaller experimental EFF and JSC can only be due to some additional recombination mechanisms not included in the computer model. This contention is further supported by the nearly ideal dark I-V slope of one, $I \propto \exp(qV/kT)$, over several decades of current, including the open-circuit voltage and short-circuit current points. One possible cause is the high emitter recombination current due to enhanced solubility of Ti in the high concentration phosphorus diffused emitter. This would be more important when the silicon is doped to a high Ti concentration since then a source of high Ti concentration is present. Enhancement of Ti solubility in the emitter was not included in the computer model used to compute the theoretical curves given in Figure 3.3. However, sample calculations were made which showed that even with an emitter lifetime of $\tau_p(0.2\mu m)=4$ ps at a distance of 0.05μm from the junction, JSC is reduced only to 10 mA/cm^2 from 12.5 mA/cm^2, the latter given in Figure 3.3(c) at a bulk Ti concentration of 3.8x10^{14} Ti/cm^3. This is still 25% higher than the experimental value of 7.7 mA/cm^2. Thus, increased emitter recombination current due to enhanced Ti solubility in the emitter appears to account for only half of the theoretical-experimental difference. Another possible source is areal inhomogeneity of the Ti concentration. This could make part of the cell area substantially higher in Ti concentration and lower in short circuit current and efficiency so that the JOC and EFF of the entire cell are considerably below that predicted using an average Ti concentration.

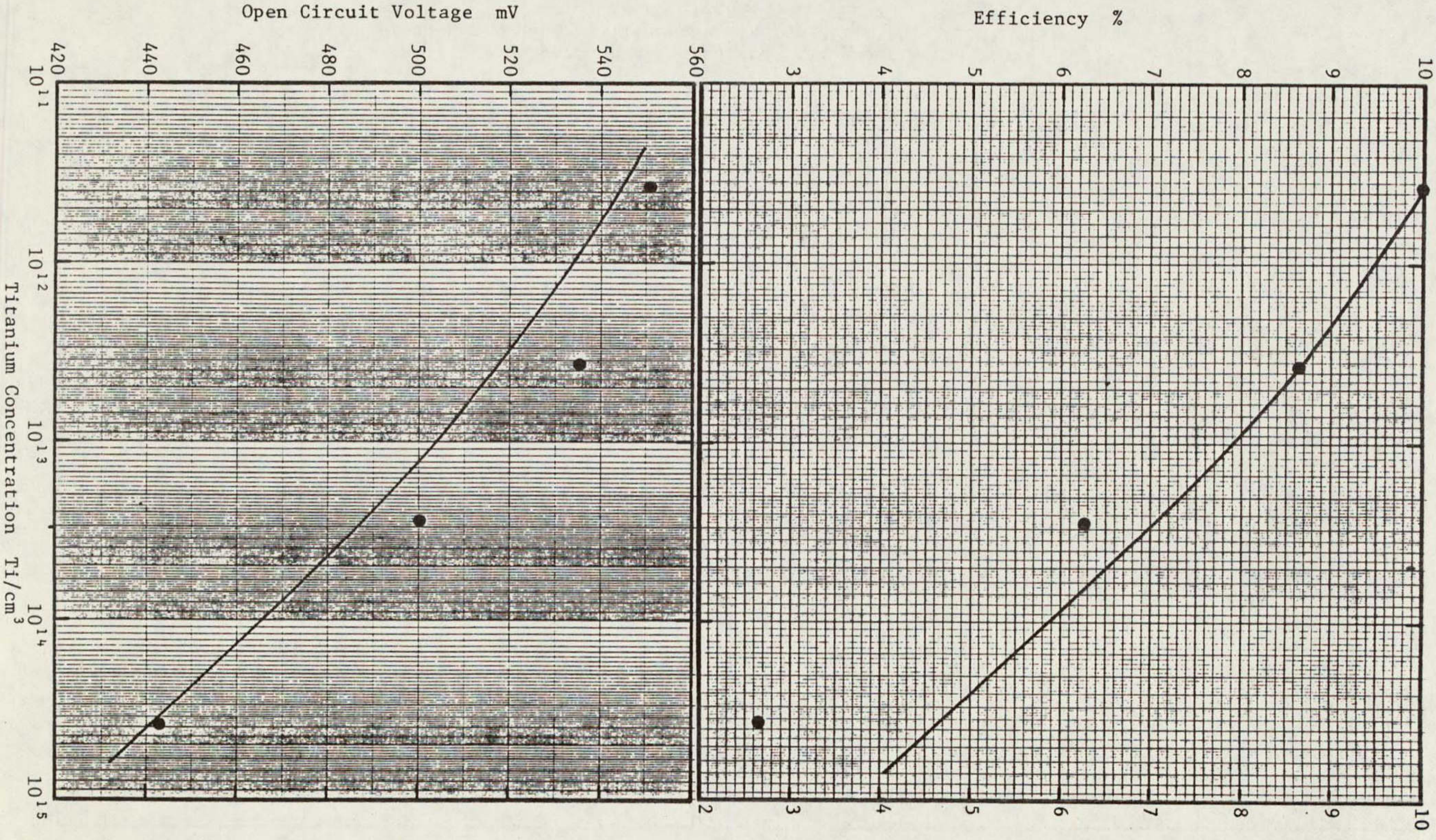

Figure 3.3 Comparison of calculated and experimental characteristics of Ti-doped p-base silicon N+/P solar cells at one AM1 sun.
(a) Efficiency, EFF
(b) Open-circuit voltage, VOC

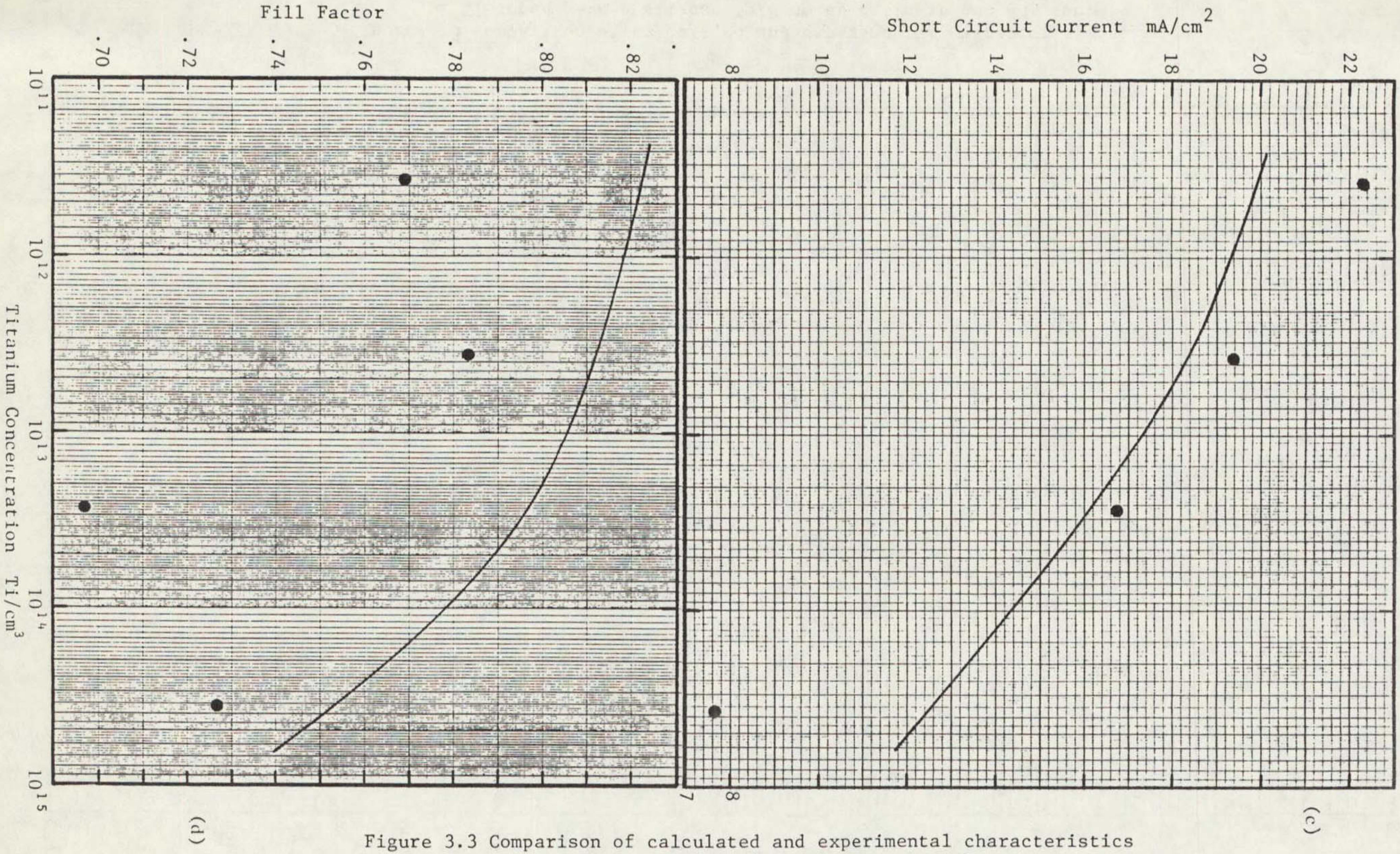

Figure 3.3 Comparison of calculated and experimental characteristics of Ti-doped p-base silicon N+/P solar cells at one AM1 sun.
(c) Short-circuit current, JSC
(d) Fill-factor, FF

3.3 Results on n-Base Cells

Very few n-type silicon doped with Ti have been grown thus far. Extensive data on cell performance have been documented only on two crystals, W065N and W121N. A comparison of theory with experiment will be made only with cells made from crystal W121N where the middle Ti donor center is believed to dominate the recombination current in the base. Computations have not been made for cells made on W065N since it was thought that the major base recombination current in this crystal is via the oxygen-vacancy or oxygen related recombination center.

The net ionized impurity concentration profile, using Table 3.4, is given by

$$N_{AA} - N_{DD} = 2.5\times10^{20}[1 - (Z/L_1)^{2/3}] - 5\times10^{15} \qquad (3.2)$$

The Ti concentration is again assumed to be spatially constant and the silicon surface reflection loss is included in the calculation. The theoretical-experimental comparison is given in the following table.

Table 3.5 Comparison of Experimental and Computed Performance of a Ti-Doped P+/N Si Solar Cell at One AM1 Sun and 4×10^{13} Ti/cm^3.

Cell No.	EFF %	VOC mV	JSC mA/cm^2	FF
W121N Expmt	7.51	525	19.9	.681
RUN733 Theory	8.54	536	17.6	.804

The agreement is fairly good considering that several experimental parameters are not accurately known and the light source used is not identical to the AM1 solar spectra. The largest difference is in the fill factor, FF. The low experimental value is probably again due to contact resistances. The slightly higher experimental JSC probably reflects the difference between the light source and the solar spectra.

3.4 Projected Maximum Performance

In view of the fairly good agreement between experimental data and theoretical prediction presented in section 3.2 and 3.3 for both the p-base and the n-base Ti-doped cells, the Ti recombination parameters given in Table 3.3 are used to compute a family of theoretical performance curves as a function of the Ti concentration. Since the hole capture rate (2.5E-8) at the upper Ti donor level (E_C-470mV) is smaller than the electron capture rate (4E-7) at the lower Ti donor level (E_V+336mV), the efficiency is expected to be higher for the n-base than the p-base cell. The highest efficiency cell would then be the P+/N/N+ geometry with back surface field and anti-reflection coating. Thus, two theoretical curves are computed, one representing the worse case of a N+/P cell without anti-reflection coating and the other, the best case of a AR/P+/N/N+ BSF cell with perfect anti-reflection coating. The efficiency of these two cases as a function of Ti concentration is given in Figure 3.4 at the one AM1 sun condition. The cell geometry and diffusion profile used are tabulated in the third column of Table 3.4.

The results of Figure 3.4 show that for an efficiency of 16%, the maximum allowed Ti concentration is about $6\text{x}10^{12}$ Ti/cm^3 in the most efficient cell geometry, i.e. the P+/N/N+ cell with anti-reflection coating. The other characteristics of this cell are: V_{OC}=576 mV, J_{SC}=30.2 mA/cm^2 and FF=0.8215.

A single point is also computed for a P+/N cell without anti-reflection coating and shown in Figure 3.4. Table 3.6 gives all the cell characteristics for the three cells at $4\text{x}10^{13}$ Ti/cm^3 concentration. The differences between the more efficient P+/N cell and the less efficient N+/P cell come from recombination in the base region. In the n-base cell of RUN731, the hole capture rate at the upper donor level, E_C-470mV, is smaller while in the p-base cell of RUN732, the electron capture rate at the lower donor level,

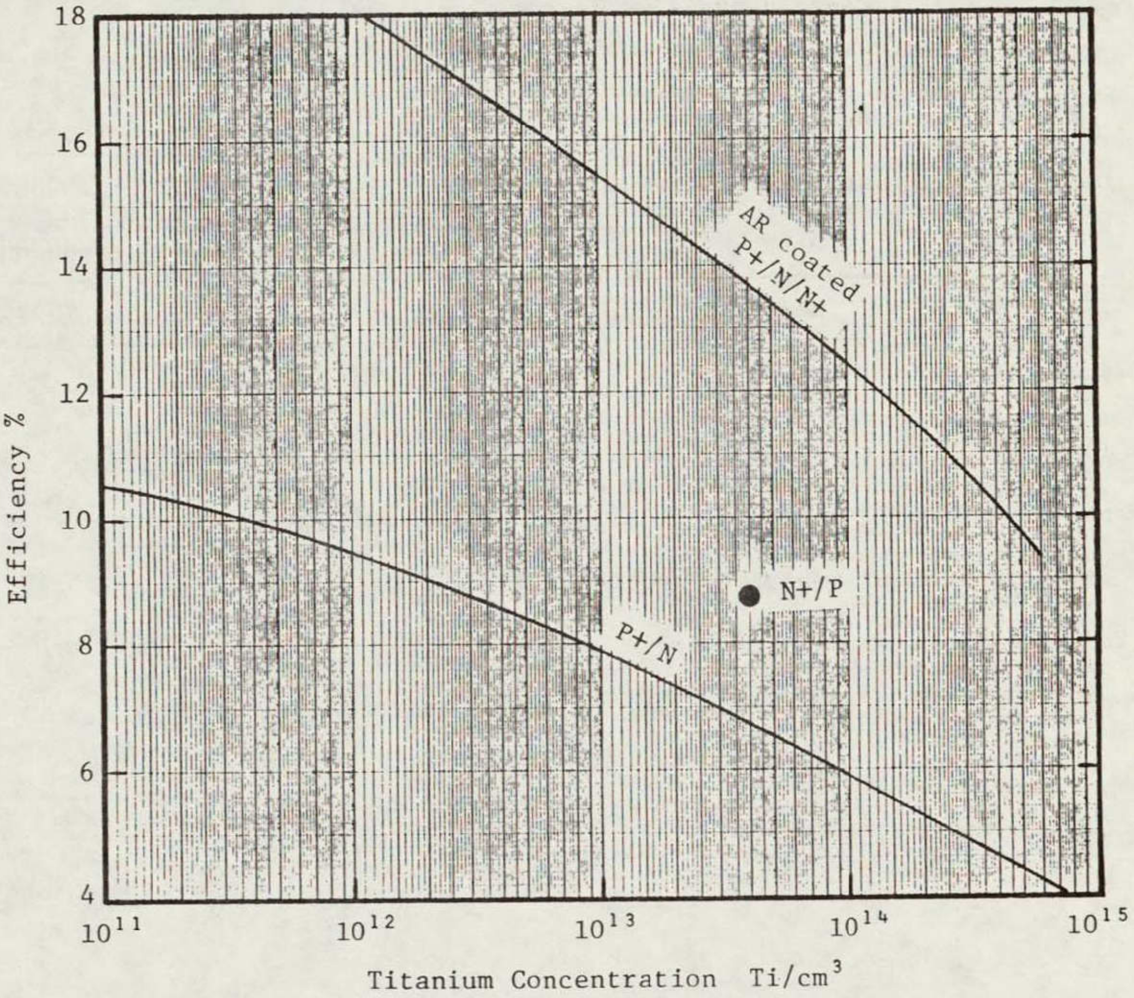

Figure 3.4 Theoretical AM1 efficiency as a function of Ti concentration for bare surface N+/P, bare surface P+/N and anti-reflection coated P+/N/N+ silicon solar cells at 297K.

Table 3.6 Performance Comparison of Bare N+/P, Bare P+/N and AR Coated P+/N/N+ Silicon Solar cells At One AM1 Sun and Containing $4x10^{13}Ti/cm^3$.

Computer Run No.	Cell Type	JPHOTO mA/cm^2	EFF %	VOC mV	JSC mA/cm^2	FF
RUN729	AR/P+/N/N+	34.198	13.691	547.85	27.479	.80869
RUN731	P+/N	22.025	8.552	536.12	17.630	.80462
RUN732	N+/P	22.025	6.708	482.49	15.595	.79271

is larger. Thus, the base lifetime in the n-base cell is larger than that in the p-base cell. High injection level effect will make the difference in lifetime smaller than the capture rate ratio of $c_n/c_p=3.7x10^{-7}/2.5x10^{-8}$ $=14.8$, using the values from Table 3.3.

4. CONCLUSION

Interband Auger recombination in the diffused emitter and back surface field layers does not affect the silicon solar cell performance significantly even if the Auger recombination rate data are in error and too small by a factor of 100. It becomes important only when the carrier concentration in these layers is higher than about 10^{20} carriers/cm^3 throughout the entire layer.

Surface recombination at the front and back surfaces has negligible effect on cell performance unless the interface recombination velocity at these surfaces lies between the diffusion velocity, 10^5 cm/s, and the effective recombination velocity, 10^3 cm/s, of the emitter and back surface field layers.

Enhanced solubility of the metallic recombination impurities in the emitter and the back surface field layers due to high phosphorus and boron concentrations in these layers can reduce the short circuit current and the open circuit voltage respectively if the solubility reaches 10% of the diffusion impurity (boron and phosphorus) concentrations.

There is little difference in solar cell performance computed from using the Gaussian diffusion profile and the measured phosphorus and boron diffusion profiles.

For the Sandia high efficiency (16.8% AM1) and high resistivity (10 Ω-cm) P+/N/N+ silicon cells, 1% of gold in the diffused emitter or 0.1% of phosphorus-vacancy or E-center in the diffused back surface field layer will account for the observed efficiency, open circuit voltage, short circuit current and fill factor. The theoretical maximum AM1 efficiency for this cell design is 19.26% when recombination in the emitter and back surface field layers is negligible. However, if recombination in the BSF layer is the limiting factor, then eliminating it entirely will only improve the efficiency by 0.1% to 16.9% and the open circuit voltage by 26 mV to 638 mV because high injection level condition would prevail in the entire base which would reduce the fill factor. On the other hand, if emitter recombination is the limiting factor, then eliminating it entirely would improve the efficiency to 19% and open circuit voltage to 660 mV.

The reported AM1 efficiency of 16.8% by Sandia is based on measurements using a solar simulator while the computed value is based on the measured solar spectra. Thus, some upward correction of the reported efficiency may be needed. This brings the reported efficiency to almost the theoretical maximum, 19%, of this cell design. Large improvement of performance cannot be expected in this cell design which already has a base lifetime of 700 μs.

Of the three energy levels detected in Ti-doped silicon and silicon solar cells, the two lower levels are donor like and related to the Ti impurity while the upper level is acceptor like and probably related to the presence of oxygen and carbon. The maximum allowable Ti concentration for a 16% AM1 efficiency is about 6×10^{12} Ti/cm^3 in the best cell type, P+/N/N+, which is the least sensitive to Ti contamination. A cell thickness of 250 μm and a base doping of 5×10^{15} phosphorus/cm^3 or a resistivity of 1.5 ohm-cm are also assumed. This cell would have an open circuit voltage of 576 mV and a short circuit current of 30 mA/cm^2.

5. REFERENCES

1. C. T. Sah
Study of the Effects of Impurities on the Properties of Silicon Materials and Performance of Silicon Solar Cell,
First Technical Report, April 1978, DOE/JPL-954685-78/1

2. Richard B. Fair
Analysis of Phosphorus-Diffused Layers in Silicon
J. Electrochemical Soc. v125, 323-327, 78FEB01

3. Richard B. Fair
Boron Diffusion in Silicon-Concentration and Orientation Dependence, Background Effects, and Profile Estimation
J. Electrochemical Soc. v122, 800-805, 75JUN01

4. J. G. Fossum and E. L. Burgess
High-Efficiency P+/N/N+ Back-Surface-Field Silicon Solar Cells
Applied Physics Lett. v33, 238-240, 78AUG01

J. G. Fossum, E. L. Burgess and R. D. Nasby
Development of High-Efficiency P+/N/N+ Back-Surface-Field Silicon Solar Cells
Proceeding of the 13th Photovoltaic Specialists' Conference, v.78CH1319-3ED, 1294-1299, IEEE, 1978

5. J. Dziewior and W. Schmid
Auger Coefficients for Highly Doped and Highly Excited Silicon
Applied Physics Lett, v13, 346-348, 77SEP01

6. C. T. Sah and F. A. Lindholm
Carrier Generation, Recombination, Trapping and Transport in Semiconductors with Position-Dependent Composition
IEEE Trans, vED-24, 358-362, 77APR01

7. C. T. Sah and W. Shockley
Electron-Hole Recombination Statistics in Semiconductors Through Flaws with Many Charge Conditions
Physical Review, v109, 1103-1115, 58FEB15

8. R. H. Hopkins, J. R. Davis, P. Rai-Choudhury, P. D. Blais, and J. R. McCormick
Silicon Materials Task of the Low Cost Solar Array Project
Second Quarterly Report, 76JAN01 to 76MAR31
Westinghouse Research Laboratories

9. R. H. Hopkins, Davis, Blais, Rai-Choudhury, Hanes, McCormick
Silicon Materials Task of the Low Cost Solar Array Project
Seventh Quarterly Report, 77APR01 to 77JUN31
Westinghouse Research Laboratories

10. C. T. Sah, unpublished. This resistivity-impurity concentration curve can be computed using the mobility formulae given on page 33 of TR-1.[1]

5. REFERENCES (continued)

11. J. C. Irving
Resistivity of Bulk Silicon and of Diffused Layers in Silicon
Bell Syst. Tech. J. v41, 387 (1962)

12. Matthews P. Thekaekara
Data on Incident Solar Energy
Journal of Environmental Science, v17, 21-49 1974

13. Jerry G. Fossum
Computer-Aided Numerical Analysis of Silicon Solar Cells
Solid-State Electronics, v19, 269-277, 1976

14. R. H. Hopkin, et.al.
Silicon Materials Task of the Low Cost Solar Array Project
Fifth Quarterly Report and Summary, 76OCT01 to 76DEC31
page 42 (DOE/JPL-954331-77/1)

15. H. Y. Tada and J. R. Carter, Jr.
Solar Cell Radiation Handbook
JPL Publication 77-56, November 1, 1977

16. Michael P. Godlewski, Cosmo R. Baraona and Henry W. Brandhorst
Low-High Junction Theory Applied to Solar Cells
Record of the 10-th Photovoltaic Specialist Conference,
IEEE Cat. No. 73CH0801-ED, 40-49, 1973

17. C. T. Sah
Detection of Recombination Centers in Solar Cells from Junction Capacitance Transients
IEEE Trans. vED-24, 410-419, 77APR01

18. N. B. Hannay
Semiconductors
Chapter 5, Defect Interactions in Semiconductors by C. S. Fuller
Reinhold Publishing Corporation, 1959

19. J. W. Walker and C. T. Sah
Properties of 1.0-MeV Electron-Irradiated Defect Centers in Silicon
Physical Review B, v7, 4587-4605, 15 May 1973

20. J. W. Walker and C. T. Sah
Characteristics of 1.0 MeV Electron-Irradiated Surface-Controlled Silicon Junction Diodes
Radiation Effects, v20, 187-195, 1973

21. R. H. Hopkins, et. al.
Effects of Impurities and Processing on Silicon Solar Cells
Fifth Quarterly Report and Summary of Phase I (DOE/JPL-954331-77/1)
Eleventh Quarterly Report and Summary of Phase II (DOE/JPL-954331-78/3)
Westinghouse Research Laboratory

5. REFERENCES (continued)

22. Henry W. Gutsche and Dale E. Hill
Determination of A definition of Solar Grade Silicon, Final Report
Monsanto Research Corporation, P.O.Box 8, St. Peters, MO 63376
ERDA/JPL 954338-76 (October 1975 to September 1976)

23. Siegfried Othmer and Susan C. Chen
Lifetime and Diffusion Length Measurements on Silicon Materials and Solar Cells
Final Report, ERDA/JPL 954614-77/1,(16DEC76 to 31OCT77)
Northrop Research and Technology Center, Palos Verdes Peninsula, CA.